PLOS ONE

RESEARCH ARTICLE

Detailed characterization of the solution kinetics and thermodynamics of biotin, biocytin and HABA binding to avidin and streptavidin

Roberto F. Delgadillo[1☯¤]*, Timothy C. Mueser[2☯], Kathia Zaleta-Rivera[3‡], Katie A. Carnes[4‡], José González-Valdez[5☯], Lawrence J. Parkhurst[1☯]*

1 Department of Chemistry, University of Nebraska—Lincoln, Lincoln, Nebraska, United States of America, **2** Department of Chemistry and Biochemistry, University of Toledo, Toledo, Ohio, United States of America, **3** Department of Bioengineering, University of California San Diego, San Diego, California, United States of America, **4** GlaxoSmithKline, Medicinal Science and Technology, R&D, King of Prussia, Pennsylvania, United States of America, **5** Tecnologico de Monterrey, School of Engineering and Science, NL, Monterrey, Mexico

☯ These authors contributed equally to this work.
¤ Current address: Tecnológico de Monterrey, School of Engineering and Science, NL, Monterrey, Mexico
‡ These authors also contributed equally to this work.
* delgadillo@tec.mx (RFD); LJP1@unl.edu (LJP)

Citation: Delgadillo RF, Mueser TC, Zaleta-Rivera K, Carnes KA, González-Valdez J, Parkhurst LJ (2019) Detailed characterization of the solution kinetics and thermodynamics of biotin, biocytin and HABA binding to avidin and streptavidin. PLoS ONE 14(2): e0204194. https://doi.org/10.1371/journal.pone.0204194

Editor: Colin Johnson, Oregon State University, UNITED STATES

Received: August 26, 2018

Accepted: February 1, 2019

Published: February 28, 2019

Data Availability Statement: All relevant data are in the paper and its Supporting Information files.

Funding: The work was supported by: National Institutes of Health Grants GM59346 and RR015468 to LJP; CONACYT-Mexico postdoctoral, SNI fellowships (130994, 162809, SNI75487) and the Government of Veracruz-Mexico gifted-student fellowships to RFD; Bioengineering, Biosystems and Synthetic Biology Focus Group of Tecnológico de Monterrey. The author K.A.C. is an employee of

Abstract

The high affinity ($K_D \sim 10^{-15}$ M) of biotin for avidin and streptavidin is the essential component in a multitude of bioassays with many experiments using biotin modifications to invoke coupling. Equilibration times suggested for these assays assume that the association rate constant (k_{on}) is approximately diffusion limited (10^9 $M^{-1}s^{-1}$) but recent single molecule and surface binding studies indicate that they are slower than expected (10^5 to 10^7 $M^{-1}s^{-1}$). In this study, we asked whether these reactions in solution are diffusion controlled, which reaction model and thermodynamic cycle describes the complex formation, and if there are any functional differences between avidin and streptavidin. We have studied the biotin association by two stopped-flow methodologies using labeled and unlabeled probes: I) fluorescent probes attached to biotin and biocytin; and II) unlabeled biotin and HABA, 2-(4'-hydroxyazobenzene)-benzoic acid. Both native avidin and streptavidin are homo-tetrameric and the association data show no cooperativity between the binding sites. The k_{on} values of streptavidin are faster than avidin but slower than expected for a diffusion limited reaction in both complexes. Moreover, the Arrhenius plots of the k_{on} values revealed strong temperature dependence with large activation energies (6–15 kcal/mol) that do not correspond to a diffusion limited process (3–4 kcal/mol). Accordingly, we propose a simple reaction model with a single transition state for non-immobilized reactants whose forward thermodynamic parameters complete the thermodynamic cycle, in agreement with previously reported studies. Our new understanding and description of the kinetics, thermodynamics, and spectroscopic parameters for these complexes will help to improve purification efficiencies, molecule detection, and drug screening assays or find new applications.

GlaxoSmithKline which provided support in the form of salary for her but did not have any additional role in the study design, data collection and analysis, decision to publish, or preparation of the manuscript. The specific roles of these authors are articulated in the 'author contributions' section.

Competing interests: We have the following interests: The author K.A.C. is an employee of GlaxoSmithKline. There are no patents, products in development or marketed products to declare. This does not alter our adherence to all the PLOS ONE policies on sharing data and materials.

Introduction

The extremely high affinity of biotin (B_7, vitamin H) for avidin (AV) and streptavidin (SAV) is widely exploited in biotechnology and biochemistry in a vast array of applications [1, 2]. It has been used in molecular biology as markers to identify functional moieties in proteins and receptors [3], and the development of bioprocessing affinity chromatography columns for the recovery of highly valued biomolecules [4]. More recently, advances in the characterization of these complexes have allowed the development of highly specific immunoassays, biosensors, and "omic" tools for disease identification and molecular mechanism elucidation [5–8]. Furthermore, B_7 and avidin-like interactions can be exploited for imaging purposes in the development of assays (such as, *in-vivo* real-time visualization of intracellular or other type of biological processes [9, 10]), and for monitoring the delivery of small molecules, proteins, vaccines, monoclonal antibodies, and nucleic acids in nanoscale drug delivery systems [11]. SAV and B_7 are used in Fluorescence Resonance Energy Transfer (FRET) [12] systems for drug High Throughput Screening (HTS) applications, commercially know as Homogeneous Time-Resolved Fluorescence (HTRF) [13–15]. Additionally, it has been suggested that these proteins function in nature as antimicrobial agents by depleting B_7 or sequestering bacterial and viral DNA [16, 17]. Questions concerning the biological importance have been appeared, as more avidin-like proteins are discovered in other species; for example, rhizavidin was discovered from proteobacterium *Rhizobium etli* [18, 19], tamavidin from the basidiomycete fungus *Pleurotus cornucopiae* [20], xenavidin from the frog *Xenopus tropicalis* [21], bradavidin from *Bradyrhizobium japonicum* [22, 23]; genes encoding for avidin related proteins have been found in chicken, *Gallus gallus*, and studied as recombinant proteins [24–31].

The monomers of AV and SAV are eight stranded anti-parallel beta-barrels with several aromatic residues forming the B_7 binding site at one end of the barrel [32]. Two monomers lie parallel to each other forming a dimer with an extensive interface and two dimers associate forming the weaker interface of the homo-tetramer. The unbound tetramer has modest thermal stability and the protein becomes highly thermal stable with ligand bound [33]. Intriguingly, the dimeric interface appears to be necessary for high affinity as two interface mutations show interesting effects on the K_D, a Trp110 to Lys mutation causes dimers of high affinity to form, and an Asn54 to Ala mutation results in only monomers, that remains monomeric with ligand bound, with a significantly reduced affinity ($K_D \sim 10^{-7}$ M) [34]. Thus, the use of monomeric avidin in affinity chromatography allows for reversible binding.

As it can be inferred, new applications for AV-B_7 related complexes will surely continue to emerge as more derivatives are characterized. However, to obtain reliable and sensitive applications, a better understanding of the thermodynamics, fluorescence behavior of the attached probes, and kinetic reaction mechanisms of B_7 and avidin-like systems are surely needed. This information can be used to improve purification efficacies, detection, drug screening assays, and to develop new nanotechnological applications. Therefore, we want to provide a more global description of the AV-B_7 and SAV-B_7 systems for bio- and nano-technological applications.

The association rate constant (k_{on}) of B_7 binding to AV has been assumed to be near diffusion limited since it was first measured by Green [35] (7.0×10^7 $M^{-1}s^{-1}$, pH 5 and 25˚C) employing a quenching experiment that required the quantification, by chromatographic separation, of un-reacted ^{14}C-biotin. Since then several widely varying k_{on} values have been reported for both AV and SAV ranging from 1×10^5 $M^{-1}s^{-1}$ to 2×10^8 $M^{-1}s^{-1}$ [20, 36–39] with error ranges below 10%.

Despite this information, the kinetic and thermodynamic parameters of the B_7 association to these AV and SAV proteins have not been studied with systematic detail. Consequently, for

this study, we asked whether the association rate constants (k_{on}) for B_7 binding to AV and SAV are truly diffusion controlled, what the association model and thermodynamic cycle that describe the reaction process are, and if there are any functional differences between AV and SAV. In this sense, we analyzed the k_{on} for B_7 binding to AV and SAV by two stopped-flow (SF) methodologies employing fluorescent dye labeled- and unlabeled-B_7 derivatives. In the first case, the association reactions were monitored with two sensing modalities: fluorescence change, F(t), and corrected fluorescence anisotropy, rF(t), under pseudo-first-order conditions as a function of temperature, concentration, and pH with the help of three dye-labeled B_7 probes: 1) biotin-4-fluorescein (BFl), 2) Oregon green 488 biocytin (BcO), and 3) biotinylated DNA labeled at the 3' end with fluorescein (B_7-DNA_{ds}*Fl-3') (Fig 1). The functional cofactor form of B_7 is biocytin (Bc) which is formed through an amide linkage between the ε-amine of lysine and carboxyl group of B_7. Modified BcO contains a significantly longer linker with respect to BFl which allows analysis of a potential steric effect in the association process, as has been reported elsewhere [40].

We also studied the effect of AV glycosylation by enzymatically removing the carbohydrate motif to compare the respective association rates with those of the untreated AV, SAV and analogous probes in other studies [20, 36–39]. To track bound tetrameric species that appeared after SF mixing at pseudo-first order reaction conditions, we show that the binding polynomial

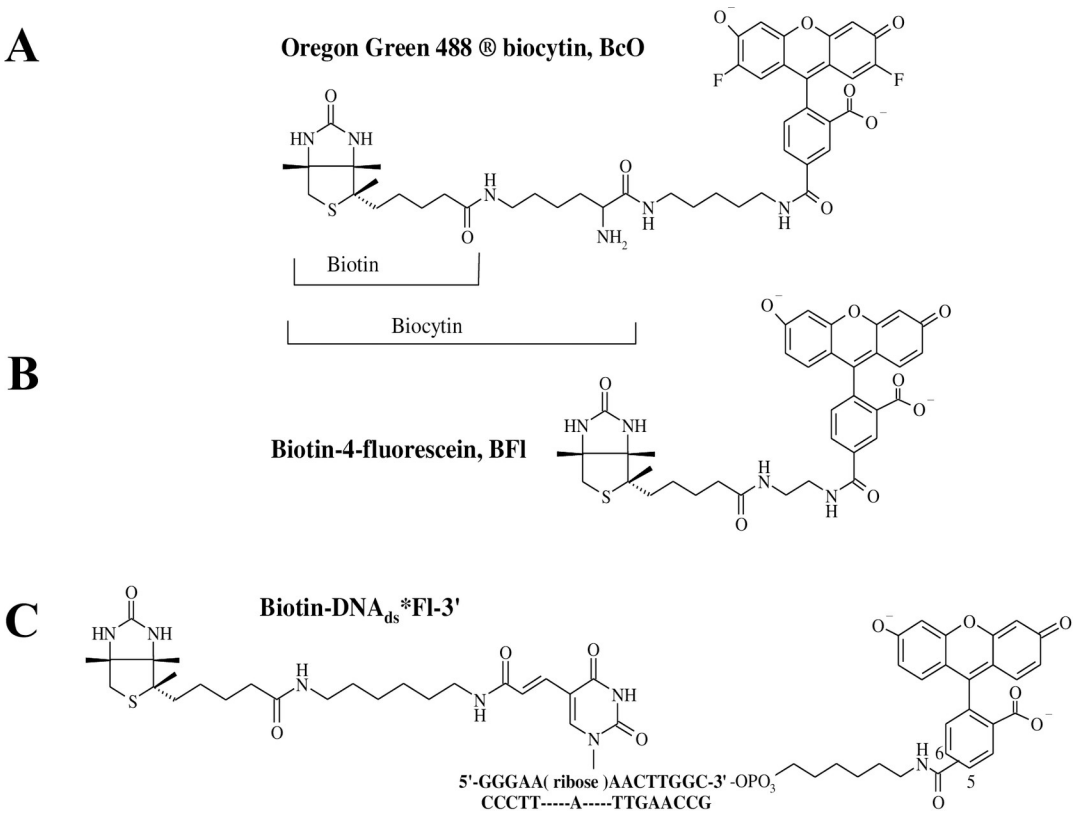

Fig 1. Dye-labeled B_7 probes. (A) Biotin-4-fluorescein (BFl) contains a shorter spacer of 10 non-hydrogen atoms between the bicyclic ring and the dye structure. **(B)** Oregon green 488 Biocytin (BcO) has a spacer of 20 non-hydrogen atoms between the bicyclic ring and the fluorescent dye. Biocytin (Bc) is an amide formed with B_7 and L-lysine. **(C)** biotinylated DNA labeled at the 3' end with fluorescein (B_7-DNA_{ds}*Fl-3'), where B_7 was attached to a 14-mer DNA duplex labeled with fluorescein (Fl) at the 3' end with 16 non-hydrogen atoms between the bicyclic ring and the thymine cyclic base. Unlabeled B_7 was used to find the reaction rate of the final binding site in AV and compare it with the reaction rates of the initial binding site to assess possible cooperativity.

https://doi.org/10.1371/journal.pone.0204194.g001

distribution (Z) allows us to know the fraction of unbound protein, and protein bounds to one, two, three and four B_7 molecules. Thus, we make a distinction of the AV and SAV complexes using a simple filling model AB_n where A is either AV or SAV, and "n" is the total available number of binding sites occupied by the dye-labeled B_7 probes and not the Hill number associated with cooperative binding.

For the second methodology, using a relaxation kinetics approach, the association reactions of unlabeled B_7 were monitored in SF instrumentation by tracking the absorbance changes of an AV-HABA complex as B_7 replaces bound HABA [41]. The presence of ligand stabilizes the avidin tetramer. AV-HABA relaxation experiments were used to determine if stabilizing the tetramer affects the association rate constants and cooperativity.

Global fitting of the kinetic traces and reported calorimetry values allowed us to test reaction models and discriminate the most probable reaction mechanism, as carried out in previous studies [42–45]. Consequently, the respective activation energies calculated by Arrhenius plots of association rates allowed the acquisition of the forward thermodynamic parameters toward the transition state: enthalpy ($E_a^{forward}$ or $\Delta H^{\ddagger, forward}$), entropy ($\Delta S^{\ddagger, forward}$) and Gibbs energy ($\Delta G^{\ddagger, forward}$) of AV and SAV activated complexes. The forward thermodynamic data is in excellent agreement with the backwards thermodynamic values calculated with the dissociation rate constants (k_{off}) reported by N. M. Green in his seminal work [35]. Additionally, we explain the nature of the second dissociation phase first observed and correctly neglected by Green as a bimolecular "displacement" rate constant ($k_{off}^{displacement}$), in addition to the detection of the documented unimolecular "replacement" rate constant ($k_{off}^{replacement}$) [26, 35] which is used to establish the well-known dissociation constant, K_D, as the most stable complex in nature.

Furthermore, we studied the changes in fluorescence lifetime (τ), quantum yield (QY), dynamic quantum yield (Φ), dye emitting fraction (1-S) and steady state anisotropy (r_{ss}) of the fluorescent probes before and after complex formation. These spectroscopic properties provide indications of the chemical environment surrounding the B_7 binding pocket in AV and SAV and have important relevance in fluorescence assay detection limits as the signal to noise ratio can be improved by carefully choosing linker length and fluorescent probe.

Experimental procedures

Materials

Probes and solution conditions. Oregon green 488 Biocytin (lot 40300A, Fig 1) was purchased from Invitrogen (Eugene, OR). Avidin (CAS 1405-69-2, lot 608540) was purchased from Calbiochem (La Jolla, CA). HABA or 2-(4'-hydroxyazobenzene)-benzoic acid (CAS 1634-82-8, lot 52F-0073), streptavidin (CAS 9013-20-1), endoglycosidase H (CAS 37278-88-9) and d-biotin (CAS 58-85-5, lot 13F-3199) were all purchased from Sigma Aldrich (St. Louis, MO). Biotin-4-fluorescein (lot 31005, Fig 1) was purchased from Biotium, Inc. (Hayward, Ca). The 3' end labeled fluorescein top strand with a modified biotinylated d-thymine at position 6 in the following sequence: `5'-GGGAA(biotin-dT)AACTTGGC*Fl-3'` (Fig 1) and the respective complement (`5'-GCCAAGTTATTCCC-3'`) were made by Tri-Link Biotechnologies, Inc. (San Diego, CA), and were both HPLC and PAGE purified. The sequences retain the G/C (base pairs) ends and fluorescein identical to those characterized extensively in our previous studies [42, 44, 46]. The biotinylated 14mer duplex (B_7-DNA_{ds}*Fl) was formed with 5-10X excess complement and incubated for at least 20 min.

Protein and active site concentrations. The AV and SAV concentrations were determined with the HABA colorimetric assay of Green [40] for which absorbance measurements, with total protein at 280 nm (1.54 = 1 mg/ml) and HABA at 500 nm (35500 $M^{-1}cm^{-1}$bound,

480 $M^{-1}cm^{-1}$unbound) were made with a Cary 300 Bio UV-Vis spectrophotometer (Varian Inc., Palo Alto, CA). The occupancy of the dye-labeled probes on the AV and SAV tetramer ("p") was obtained with the expansion version of the normalized partition function, $Z = (p + q + x)^4$. In considering the totality of binding sites in the AV and SAV tetramer, let "p" denote the fraction of total sites occupied by B_7 ligands (or HABA), "q" the fraction that are unoccupied and are available for binding, and "x" the fraction that are unavailable. The normalized partition function that describes the mole fractions of the various possible AV and SAV tetrameric species is given by $Z = (p + q + x)^4$; where "x", from the HABA assay for AV, was found to be 0.185 (or 18.5%), and q = 1—p—x. Knowing the total concentration of binding sites from UV protein absorbance and Green's methodology [40], and determining "x", results in the maximum value of "p" that will be reached in reacting tetramers with a B_7 analog. Expansion of Z provides the mole fractions of the various species in solution, and in decreasing order in terms of probe occupancy, are: $p^4 + 4p^3q + 4p^3x + 6p^2q^2 + 6p^2x^2 + 12p^2qx + 4pq^3 + 4px^3 + 12pq^2x + 12pqx^2 + q^4 + x^4 + 4q^3x + 4qx^3 + 6q^2x^2$ which totals 1. This development assumes completely random occupancy of probe and inactive sites characterized by "x". The species containing one bound probe have "p" raised to the first power; those with two bound probes have "p" raised to the second power, and so on.

All of the following protein concentrations are presented on a binding site basis, thus in the case of the HABA association reactions for AV were measured at 23.0 ± 0.1˚C with a concentration of 87 μM HABA and 7.7 μM AV. The AV-HABA relaxation reactions were conducted with a preformed AV-HABA complex made up of 200 μM HABA and 10 μM AV, flowed against varying amounts of B_7 from 100 μM up to 4000 μM for a [HABA]/[B_7] ratio that ranged from 0.05 to 2.

Association stopped-flow kinetics. These reactions were carried out in a buffered solution of 10 mM Tris-HCl, 100 mM KCl, 2.5 mM $MgCl_2$ and 1 mM $CaCl_2$ at pH 8 and only AV-BcO reactions included pH 9 and 10. The concentrations, after mixing, were of 20 nM of dye-labeled B_7 probe and 260 nM, 520 nM or 1040 nM of AV; and 200 nM, 300 nM, 400 nM or 800 nM of SAV at temperatures of 10, 15, 20 and 25˚C. The deglycosylation of AV (for comparative association reactions) was carried out using the provided standard protocol with endoglycosidase H [47], both with and without incubation of a denaturant solution (2% SDS and 1M 2-mercaptoethanol).

Dissociation reactions of dye-labeled biotin complexes. Biotin dissociation was determined using labelled biotin (BcO and BFl) displaced by unlabeled biotin using minimally occupied and fully occupied binding sites. In the minimally occupied measurements, SAV is prepared with less than one site on average occupied by labelled biotin (AB_1), using 800 nM SAV and 40 nM of BcO or BFl. For saturated SAV-labelled biotin (AB_4) complexes, equimolar binding sites and labelled ligand were prepared, 40 nM SAV and 40 nM of BcO or BFl. The AB_1 complexes were challenged in displacement experiments with several concentrations of unlabeled B_7 (1500 nM, 1750 nM, 2000 nM and 2500 nM) at 20 ± 0.1˚C. In AB_1, SAV had 760 nM in open sites, therefore the total challenging B_7 concentrations were 740 nM, 990 nM, 1240 nM and 1740 nM, respectively. Additional measurements at 27 ± 0.1˚C using 1300 nM, 1500 nM, 1750 nM, 2000 nM and 3000 nM biotin were completed. The 40 nM AB_4 complexes were challenged with unlabeled B_7 concentrations of 400 nM (10X) and 1600 nM (40X) at 20 ± 0.1˚C. The dissociation reactions of AV complexes were carried out with a preformed complex of 20 nM BFl or BcO and 260 nM AV for a filling model of AB_1 and challenged with unlabeled B_7 at 2,000 nM.

Spectroscopic properties. The lifetimes (τ), steady state anisotropies (r_{ss}), time-resolved anisotropies (r_t) and quantum yields (QY) of the complexes (at 20 ± 0.1˚C and pH 8) were collected with a dye-labeled B_7 probe concentration of 20–40 nM and 1040–2080 nM of either

protein (AV or SAV) to ensure that only one binding site in the tetramer was filled with a ligand (AB_1 filling model).

Methodologies

The following experiments were carried out by at least six times, unless indicated, and the reported errors correspond to the standard deviation.

Steady-state anisotropy (r_{ss}). The r_{ss} measurements were collected using the Giblin-Parkhurst modification of the Wampler-Desa method as described previously [48]. The fluorescence signal was detected in a model A-1010 Alphascan fluorimeter (Photon Technologies, Inc., Birmingham, NJ) equipped with an R928 PMT (Hamamatsu, Bridgewater, NJ). The excitation was provided by an Ar^+ ion laser (Coherent Innova 70–4 Argon, Santa Clara, CA) at 488 nm and 5–10 mW of power incident on the sample. A photoelastic modulator (PEM-80; HINDS International, Inc., Portland, OR) was placed between the laser source and the sample compartment with a retardation level of 1.22π, and the PEM stress axis orientated 45˚ with respect to the E vector of the laser beam. Two signals were acquired with the PEM alternating between "on" and "off" positions for 10 seconds and the data fitted to a least squared straight line to minimize noise. A minimum of six of these independent measurements were averaged to acquire the r_{ss} values. The fluorimeter G factor was determined using a film polarizer and analyzer with an excitation at 488 nm provided by a xenon arc lamp (model A1010, Photon Technologies Inc, Princeton, NJ). The dissociation reactions of dye-labeled B_7 and protein complexes were monitored by fluorescence changes and were also collected in the fluorimeter described above.

Fluorescence lifetimes (τ) and time-dependent anisotropy decays (r_t). The lifetimes were collected in a FluoTime100 fluorescence spectrometer (PicoQuant, GmbH, Berlin, Germany) with the excitation light source provided by a picosecond pulsed diode laser (PicoQuant, GmbH, Berlin, Germany) at 470 nm and 20 MHz. The emission was collected at 520 nm through a non-fluorescing 520 nm interference filter (Oriel Corp., Stratford, CT) followed by a liquid filter of 1cm path length containing 24 mM acetate buffered dichromate at pH 4, between the sample and detector to eliminate traces of excitation light [42]. The fluorescence decays were fit by a nonlinear least-squares minimization based on the Marquardt algorithm embedded in the Fluofit software (PicoQuant GmbH). Twenty-eight decays were collected per sample, the decays were grouped in four sets, consisting of seven sample decays and one Instrument Response Function, IRF, for deconvolution proposes. The decay sets were globally fitted to mono- or bi-exponential decay models that were discriminated using the statistical parameter χ^2. The r_t data were acquired with the fluorimeter described above equipped with a polarizer and an analyzer to acquire the parallel VV(t) and perpendicular VH(t) decays. The PicoQuant G factor was calculated according to: $G = \int HV(t)dt / \int HH(t)dt$, where HV(t) and HH(t) were the decays collected with the emission polarizer selecting vertical and horizontal E-vector passing orientations, respectively, and the excitation polarizer set at horizontally position.

Quantum yields (QY). The QY values were obtained by using a reference fluorophore of known quantum yield and were calculated according to Parker and Rees [49, 50], where the reference dye was fluorescein in 0.1N sodium hydroxide solution [46]. The emission fluorescence scans were collected from 480 nm to 700 nm with the excitation light set at 460 nm provided by the xenon arc lamp described above. These measurements were made on the AB_1 complexes at high protein concentration.

Intrinsic lifetime (τ˚), dynamic quantum yield (Φ) and fraction of non-statically quenched molecules (1-S). These calculations have been described elsewhere [46] and were

acquired for the AB_1 complexes. The HABA association reaction for AV was carried out under pseudo-first order conditions on a micro absorbance SF instrument [51] equipped with a xenon arc lamp (described above) and a monochromator (model 82–410, Jarrel-Ash, Waltham, Mass.) set at 500 nm.

Relaxation kinetics of unlabeled biotin reacting with the AV-HABA complexes. The relaxation experiments were prepared at concentrations in which HABA occupies all sites (AV-$HABA_4$). Biotin replaces HABA relative to the k_{off} of the dye as shown for the first step (Eq 1) and then repeated for all sites. Having greater affinity, B_7 occupies all sites at the end of the reaction and the measured k_{on} is related to the affinities of the ligand bound protein.

$$AV{-}HABA_4 + B_7 \underset{k_1^{AV-HABA3}}{\overset{k_{-1}^{AV-HABA4}}{\rightleftarrows}} AV{-}HABA_3 + HABA + B_7 \xrightarrow{k_{on}^{B}} (B_7{-}AV{-}HABA_3) + HABA \quad (1)$$

The reaction is monitored by the HABA absorbance changes at 500 nm as it is replaced by unlabeled B_7; yielding the relaxation constant of the reaction (Relaxation, Eq 2) which contains information of the B_7 association rate constant of the open binding site, $k_1^{AV-HABA3}$ to form a full saturated complex (AV-$HABA_4$) and the dissociation rate of that full complex, $k_{-1}^{AV-HABA4}$, to yield a complex with three HABA molecules (AV-$HABA_3$). In the subsequent steps, B_7 replaces HABA as the ligand but the release of HABA creates an unoccupied site that remains in the same state. In summary, the experiment was designed to acquire the pseudo-first order association rate constant of B_7 binding (k_{on}^{B}) to the solely free binding site in a complex occupied by three HABA molecules (AV-$HABA_3$).

$$Relaxation = \frac{k_{-1}^{AV-HABA4} \cdot k_{on}^{B} \cdot [B_7]}{[HABA] \cdot k_1^{AV-HABA3} + k_{on}^{B} \cdot [B_7]} \quad (2)$$

The reciprocal of the relaxation constant (1/Relaxation) is plotted vs. the [HABA]/[B] concentration ratio (Eq 3) allowing to calculate: $k_{-1}^{AV-HABA4}$ and $k_1^{AV-HABA3}$ by solving for the intercept ($1/k_{-1}^{AV-HABA4}$) and the respective slope: $m = k_1^{AV-HABA3}/(k_{-1}^{AV-HABA4} \cdot k_{on}^{B})$. The exponential decays were analyzed by the method of Foss [52]. There was no departure from simple first order decay in the relaxation, justifying the use of the following model and equations.

$$\frac{1}{Relaxation} = \frac{k_1^{AV-HABA3} \cdot [HABA]}{k_{-1}^{AV-HABA4} \cdot k_{on}^{B} \cdot [B_7]} + \frac{1}{k_{-1}^{AV-HABA4}} = m \cdot \frac{[HABA]}{[B_7]} + \frac{1}{k_{-1}^{AV-HABA4}} \quad (3)$$

Association reactions of dye-labeled biotin and AV (or SAV). The reactions were collected with the SF instrument, described previously [53, 54]. The fluorescence signal was collected through a 520 nm interference filter (Oriel Corp., Stratford, CT) with a detector time constant and SF dead time of 1 μs and 1 ms, respectively. The excitation light was provided by the Coherent Ar^+ ion laser (described above) at 488 nm with 15–10 mW of incident power on the reaction cuvette. The laser source was followed by the photo-elastic modulator described above with the axis oriented 45° with respect to the electric vector of the incident light and with the half-wave modulation (50 kHz) set for 488 nm excitation. The demodulation circuitry following the photomultiplier provided a DC(t) and a rectified AC(t) which were converted to digital data by a high-speed digitizer (PCI-5122) from National Instruments (Austin, TX) with 14-bit resolution and 100 MHz bandwidth, through channels 0 and 1. The data acquisition was controlled by LabVIEW (Vr 8) software at a collection rate of 6120 data points/second and stored in spreadsheets. The AC(t) and DC(t) data were baseline corrected before obtaining the

signal ratio (Eq 4) as a function of time (ρ_t).

$$\rho(t) = \frac{AC(t)}{DC(t)} = \frac{1.5 \cdot r(t) \cdot A_{Gain}}{1 - 0.47818 \cdot r(t) \cdot (1 + 2.3806 \cdot H)} \quad (4)$$

The constant A_{Gain} is the instrumental amplitude gain and was evaluated by solving ρ(t) using the known steady state anisotropy (r_{ss}) of the complexes which is equivalent to the r(t) at t = ∞; and H, obtained from the equivalent grating factor (G) for the filters and photo multiplier tubes in the SF. For the probes used in here G was 0.82 and H = (1-G)/(1+G) = 0.099. Knowing A_{gain} and H, the AC(t) and DC(t) signals can be solved for $r(t)$ and $F(t)$ (Eqs 4 and 5) and the normalized fluorescence, $\overline{F}(t)$, and corrected fluorescence anisotropy, $\overline{rF}(t)$ [55], were obtained when $\overline{F}(0)$ and $\overline{rF}(0)$ were scaled to 1 at t = 0.

$$F(t) = \frac{DC(t)}{1 - 0.47818 \cdot r(t) \cdot (1 + 2.3806 \cdot H)} \quad (5)$$

The $\overline{F}(t)$ (Eq 6) is equivalent to ($I_{||}$) + 2 ($I_{\perp}$) and proportional to quantum yield (QY_i), molar absorptivity (ε_i) and to the formation or disappearance of the emitting species $X_i(t)$; and $\overline{rF}(t)$ including the steady state anisotropies (r_{ss}) of each fluorescent species (Eq 7) [55].

$$\overline{F}(t) = \sum \varepsilon_i \cdot QY_i \cdot X_i(t) / \sum \varepsilon_i \cdot QY_i \cdot X_i(0) = F(t)/F(0) \quad (6)$$

$$\overline{rF}(t) = \sum \varepsilon_i \cdot r_{i,ss} \cdot QY_i \cdot X(t)_i = rF(t)/rF(0) \quad (7)$$

Biotin association reaction model for AV and SAV. The possible reaction models were discriminated by the squared residuals of the observed and calculated association traces of both fluorescence and anisotropy fluorescence signals, $\overline{F}(t)$ and $\overline{rF}(t)$, respectively. For the BFl and BcO probes, the association reactions were very well described by the simplest possible model (Eq 8) with single association rate constants (k_{on}).

$$AV(or\ SAV) + Dye{-}labeled\ B_7 \xrightarrow{k_{on}} Complex \quad (8)$$

In the case of the B_7-DNA_{ds}*Fl, the association reaction model was complemented by a second k_{on} which resulted in a system of two parallel reactions (Eq 9). In both cases, the backward reaction is not significant during the 5–8 sec required for the B_7 association binding.

$$\begin{matrix} AV(or\ SAV) + (B_7{-}DNA_{ds}{}^{*}Fl)_1 \xrightarrow{k_{on1}} \\ AV(or\ SAV) + (B_7{-}DNA_{ds}{}^{*}Fl)_2 \xrightarrow{k_{on2}} \end{matrix} Complex \quad (9)$$

Dissociation reactions of the complexes. The dissociation reactions were followed by fluorescence changes, $\overline{F}(t)$, in the fluorimeter and laser setup described above and tuned to 488 nm under discontinuous excitation to prevent photobleaching distortion. The signal was best fitted to the following dissociation model (Eq 10), in which the dye labeled complex dissociates into the labeled B_7 probe (BFl or BcO) and the respective protein (AV or SAV).

$$\begin{matrix} Complex\ (dye - labeled\ B_7) + B_7 \xrightarrow{k_{off}^{displacement}} \\ Complex\ (dye - labeled\ B_7) + B_7 \xrightarrow{k_{off}^{replacement}} \end{matrix} AV - B_7\ (or\ SAV - B_7) + Dye{-}labeled\ B \quad (10)$$

Time-resolved anisotropy ($\overline{r}_t$). The $\overline{r}_t$ values were calculated according to Eq 11 where the pre-exponential "*f*" corresponds to the slow phase that derives from the lifetime of the

global motion (τ_G) [56] which was fitted within a range of expected correlation time for the complex size [57]; consequently, facilitating resolution of the fast correlation lifetime (τ_p) and the corresponding pre-exponential (1-*f*).

$$\overline{r}(t) = (1-f)\cdot exp\left(-\frac{t}{\tau_p}\right) + f\cdot exp\left(-\frac{t}{\tau_G}\right) \tag{11}$$

The *f* parameter was constrained to the observed r_{ss} (Eq 12) where $\hat{F}(t)$ (Eq 13) is normalized ($\alpha_1 + \alpha_2 = 1$) and derived from the observed fluorescence decays of the complex [58].

$$r_{ss} = 0.4\int \overline{r}(t)\cdot \hat{F}(t)dt \tag{12}$$

Where

$$\hat{F}(t) = \frac{\alpha_1 exp\left(-\frac{t}{\tau_1}\right) + \alpha_2 exp\left(-\frac{t}{\tau_2}\right)}{\alpha_1\tau_1 + \alpha_2\tau_2} \tag{13}$$

In a simple model, the transition moment is assumed to wobble within a cone of semi-apical angle Ω [59], where the cone axis is normal to the surface of a sphere that corresponds to the macromolecule. The angle Ω is calculated from Eq 14.

$$f = \left[\frac{1}{2}cos\Omega(1+cos\Omega)\right]^2 \tag{14}$$

Results and discussion

Active avidin binding sites

The avidin and streptavidin proteins are tetramers in solution. If the binding of the ligand is positively cooperative, differences in k_{on} for initial and final binding steps could be significant; therefore, the comparison of initial binding by nonliganded AV and final binding by liganded AV is necessary. Measurement of the initial binding rate requires ligand free AV, but endogenous ligand could potentially interfere. In fact, AV preparations often present about 20% of the inactive sites for the binding of any B_7 analogs, either because they contain endogenous B_7 [40], or perhaps the existence of damaged binding sites in some of them, *e.g.*, tryptophan oxidation [60]. To acquire accurate k_{on} values, the actual available binding site concentration for each sample was measured by HABA colorimetric assays in relation with absorbance at 280 nm. Accordingly, the percentage of available active sites of AV and SAV were 81.5 ± 1.0% and 94.0 ± 1.0% with respect to total protein, respectively, which were in excellent agreement with the 82% and 95% reported by the commercial source (Sigma Aldrich and CalBiochem). The SF apparatus provided rapid thorough mixing of the probes with AV and SAV allowing measurement of the full reaction. The issue of rapid mixing *vs.* more conventional titrations was treated previously [51]. In the SF association measurements, the dye-labeled B_7 probes were sub-stoichiometric to determine the initial binding rates (e.g. 20 nM of BFl, BcO and B_7-DNA_{ds}*Fl vs. 260 nM, 520 nM and 1040 nM in binding sites basis). Limiting the ligand also reduced several potential measurement artifacts including FRET self-transfer, and contact interference including probe fluorescence quenching by contact interactions [61] in the AB_2, AB_3 or AB_4 complexes; especially for the BcO which has a longer linker [62]. Using the binding polynomial for the 20 nM probe after mixing, and 638 nM in total sites for the intermediate AV concentration which corresponds to 520 nM in available sites, the mole fraction of species with a single bound probe is 0.114, that with two bound probes is 0.0055, and with three bound probes is 0.0001, so at most, only 0.55% of the molecules with bound AV contain two

probes; for 1040 nM available sites, the value drops to 0.15% (S1 File). With limited occupancy, the association reactions acquired the dye-labeled B_7 probes reflect the binding to the first binding site in the tetramer for the SF experiments. The unlabeled B_7 relaxation kinetic experiment was designed to observe the binding at the final site, as discussed below.

Association rate constants (k_{on}) of biotin binding to avidin

Dye-labeled biotin association rate constants by stopped-flow methodology. The fluorescence $\overline{F}(t)$ and corrected anisotropy association binding traces, $\overline{rF}(t)$, properly monitored the association reactions, as they yielded equivalent k_{on} values (Table 1) and presented the best optimal fit residuals (Fig 2). In contrast, the anisotropy signal, $\overline{r}(t)$, lagged behind $\overline{F}(t)$ and $\overline{rF}(t)$ since changes in the quantum yield (QY) of the involved fluorescence species distort the kinetic traces [55]. These three types of association binding traces were acquired with discontinuous excitation that circumvented photobleaching (Fig 3) allowing the detection of all non-photobleaching rate constants. Consequently, the k_{on} values of AV showed linear concentration dependence (Fig 4) and strong temperature dependence when using the BcO (Fig 5) and BFl (Table 2) probes. Notably, a reduction in the k_{on} of ~10% was observed with each pH unit increment (from 8 to 10) which may derive from titration of the hydrogen bonding of asparagine and tyrosine in the binding pocket [32].

Unlabeled biotin association rate constants by relaxation kinetics methodology. The experiment consisted in challenging a pre-saturated AV-HABA complex with B_7 (Fig 6) to measure the association rate of the final "relaxed" binding sites which yielded a k_{on}^{B} of $5.3 \pm 0.9 \times 10^6$ $M^{-1}s^{-1}$ (at pH 8 and 23˚C) which is slightly slower than the $7.8 \pm 0.4 \times 10^6$ $M^{-1}s^{-1}$ acquired with BcO (Arrhenius plot, 23˚C and pH 8) indicating non-cooperativity (or slightly negative) for binding site association rates. The HABA dissociation rate constant of the AV-$HABA_4$ complex was not rate limiting ($k_{-1}^{AV-HABA4} = 6.23 \pm 0.11$ s^{-1}) and the HABA association rate for the final site was $k_{1}^{AV-HABA3} = 5.1 \pm 0.1 \times 10^5$ $M^{-1}s^{-1}$ which results in a AV-HABA equilibrium constant of $K_D^{\text{AV-HABA}} = 12.2 \pm 0.3 \times 10^{-6}$ M similar to that reported by Green [60] at pH 8 which supports the quality of our relaxation kinetic experiment.

Non-cooperative biotin binding to avidin sites. The association reactions that used the fluorescent probes BFl and BcO monitored the 1st available binding site, as they were carried out at pseudo-first order, at very high protein concentration with low occupancy for the AB_1 filling model, as discussed above. In contrast, the relaxation kinetic methodology scrutinized the unlabeled B_7 binding to the unoccupied site while the 3 remaining sites were filled with HABA, this process can be thought as the binding of B_7 to the 4th binding site. Therefore, the data obtained with dye-labeled B_7 probes and unlabeled B_7 should report the binding rates to

Table 1. Comparison of the AV-BcO association rate constants (k_{on}) obtained by fluorescence change, $\overline{F}(t)$, and corrected fluorescence anisotropy, $\overline{rF}(t)$.

k_{on} AV-BcO	$\overline{F}(t) \times 10^{-6}$ $M^{-1}s^{-1}$			$\overline{r}F(t) \times 10^{-6}$ $M^{-1}s^{-1}$		
Temp.	**260 nM**	**520 nM**	**1040 nM**	**260 nM**	**520 nM**	**1040 nM**
25˚C	9.5 ± 0.1	9.5 ± 0.3	9.7 ± 0.3	9.5 ± 0.1	9.5 ± 0.1	9.4 ± 0.2
20˚C	5.7 ± 0.1	5.9 ± 0.3	6.0 ± 0.1	5.9 ± 0.1	5.8 ± 0.1	6.1 ± 0.1
15˚C	4.1 ± 0.1	4.0 ± 0.1	3.9 ± 0.2	4.0 ± 0.1	3.8 ± 0.1	4.0 ± 0.2
10˚C	2.4 ± 0.1	2.6 ± 0.2	2.5 ± 0.2	2.7 ± 0.1	2.7 ± 0.1	2.7 ± 0.1

The association reactions were acquired with BcO (20 nM) binding to AV at several temperatures, protein concentrations and pH 8.The $\overline{F}(t)$ and $\overline{rF}(t)$ signals were equivalent as they tracked in the errors the association process of dye-labeled B_7 binding to the proteins under pseudo-first order conditions.

https://doi.org/10.1371/journal.pone.0204194.t001

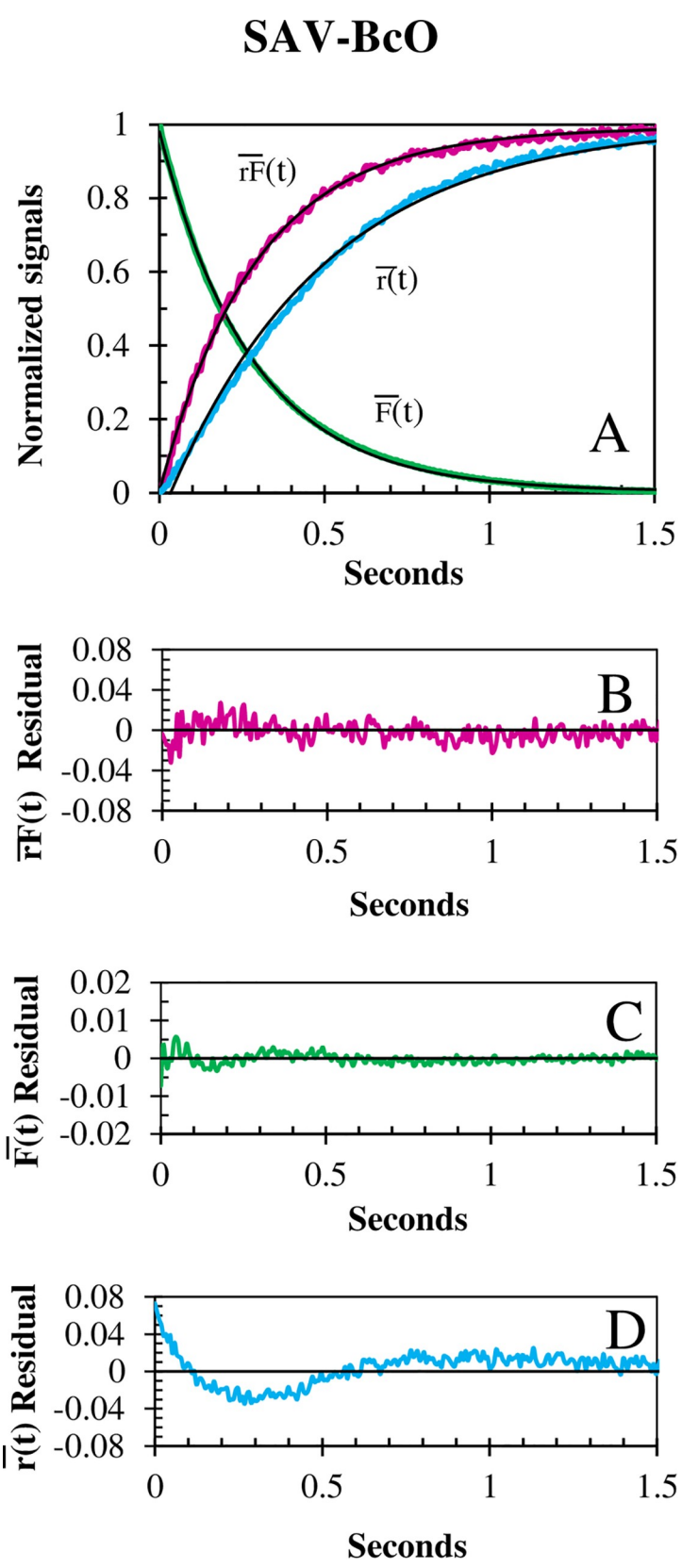
SAV-BcO
Normalized signals
rF(t)
r(t)
F(t)
A
Seconds
rF(t) Residual
B
Seconds
F(t) Residual
C
Seconds
r(t) Residual
D
Seconds

Fig 2. Comparison of the association kinetic traces. (A) Fluorescence, $\overline{F}(t)$, anisotropy, $\overline{r}(t)$ and corrected fluorescence anisotropy, $\overline{rF}(t)$ reaction traces of BcO (20 nM) binding to SAV (200 nM) at 10˚C. The mono-exponential fits (black) resulted in k_{on} values of 1.73×10^7 $M^{-1}s^{-1}$, 1.72×10^7 $M^{-1}s^{-1}$ and 1.04×10^7 $M^{-1}s^{-1}$ with halftimes of 200.6 ms, 201.4 ms and 332.7 ms, respectively. The respective residual of the reaction traces versus fit curves show that **(B)** $\overline{rF}(t)$ and **(C)** $\overline{F}(t)$ were optimal, and **(D)** $\overline{r}(t)$ signal is ill-fitted. The k_{on} of $\overline{r}(t)$ was 40% slower than the other two and showed the worst residuals due to changes in QY [55]. The corresponding normalization signals are: $\overline{rF}(t) = [rF(0) - rF(t)]/[rF(0) - rF(\infty)]$, $\overline{F}(t) = \frac{F(t)}{F(0)} = [F(t) - rF(\infty)]/[rF(0) - rF(\infty)]$ and $\overline{r}(t) = [r(0) - r(t)]/[r(0) - r(\infty)]$.

https://doi.org/10.1371/journal.pone.0204194.g002

the 1st and 4th sites. Since these two values only diverge by 32% we believe that there is not significant cooperativity nor an intrinsic difference in any of the AV sites. If a protein has two forms, denoted as relaxed (R) and tense (T), the HABA bound ligand can hold the AV protein in the R-state [63]. In the relaxation experiments, all the bound HABA gets replaced by dye-labeled B_7 (BFl or BcO), but all the sites rest in the R-state; therefore, there is not switching from T to R. This is the same as hemoglobin bound to (HbO_2) flowed against CO, where O_2 gets replaced by CO but is not biphasic because no T-state is present [63, 64]. As B_7 binding to AV and SAV is non-cooperative, the HABA replacement is a pseudo first order measure of the B_7 association rate and should be the same or close to the association rate of the dye-labeled B_7 flowed against empty AV or SAV. Our values differed only by 32% for these two approaches.

Comparisons with other AV-B kinetic studies. Comparisons with other AV-B_7 kinetic studies were carried out at the closest possible condition; thus, at 25˚C and pH 8, the BFl and BcO association rate constants, k_{on}, were 3.8X and 7.4X slower than the 7×10^7 $M^{-1}s^{-1}$ reported by N. M. Green [35] (at 25˚C and pH 5), respectively. However, a larger uncertainty is expected for the latter experiment because it was not carried out using rapid mixing techniques forcing the usage of very low (^{14}carbon) B_7 concentrations (picomolar range) to timely stop the reaction and quantify the un-reacted probe. Consequently, Green's experiment was an extremely tedious task that was carried out, only once and at one temperature. On the other hand, a more recent association rate constant of $2.0 \pm 0.3 \times 10^6$ $M^{-1}s^{-1}$ was obtained in a

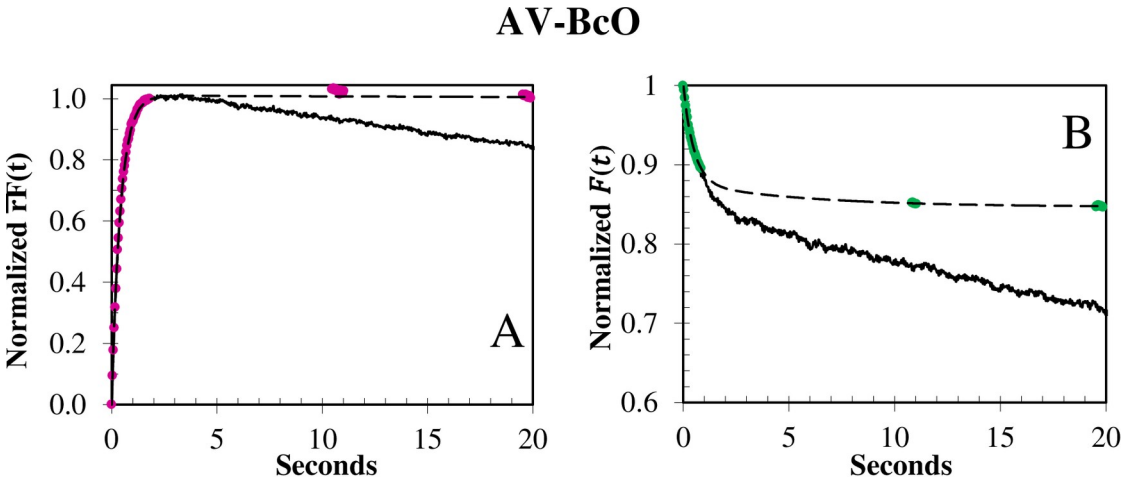

Fig 3. Photobleaching of BcO binding to AV at 15˚C. The photobleaching rate constant was elucidated with the **(A)** $\overline{rF}(t)$ and **(B)** $\overline{F}(t)$ signals by collecting the reaction with continuous (black) and discontinuous (dashed color) laser illumination in which the beam was blocked during the times denoted by dashes and the sample was illuminated only during time intervals of 10 s. The slow photobleaching rate constant varied from 6×10^{-3} to 1×10^{-2} s^{-1}, and was laser power dependent. The (A) $\overline{rF}(t)$ and (B) $\overline{F}(t)$ normalization functions were: $\overline{rF}(t) = [rF(0) - rF(t)]/[rF(0) - rF(\infty)]$ and $\overline{F}(t) = \frac{F(t)}{F(0)} = [F(t) - rF(\infty)]/[rF(0) - rF(\infty)]$, respectively.

https://doi.org/10.1371/journal.pone.0204194.g003

Surface Plasmon Resonance (SPR) study [20] at 20˚C and pH 7.4 in HEPES buffer. This independent k_{on} value was ~9X and ~5X slower than the ones acquired by us for BFl and BcO, respectively. Nevertheless, it has been previously acknowledged that the SPR results are, controversially, too low to be accurate [20, 39], due to fixation of one of the reactants to the chip, generally AV or SAV.

Effect of AV glycosylation on the biotin binding kinetics. The AV protein has a glycan attached to asparagine 17 at each tetrameric subunit which is composed of four or five mannoses and three N-acetylglucosamines [65]. These sugar modifications are typically removed to improve crystallization but the glycan effect on the association binding rate of B_7 was previously unknown. Interestingly, after enzymatic removal of the carbohydrates, the k_{on} values of the de-glycosylated AV matched those of natural glycosylated AV for the dye-labeled B_7 probes: e.g., $3.7 \pm 0.3 \times 10^{-6}$ $M^{-1}s^{-1}$ vs. $3.9 \pm 0.3 \times 10^{-6}$ $M^{-1}s^{-1}$ of BcO binding to de-glycosylated AV and untreated AV at 15˚C, respectively. A previous study already suggested that the sugar chain is not required for B_7 binding [65] and now we confirm that AV glycosylation has no influence on the association rate constants.

Association reaction of unlabeled and dye-labeled biotin binding to streptavidin

Dye-labeled biotin association reactions to SAV. The SAV-B_7 association reactions presented temperature (Fig 4C and 4D) and linear concentration dependence (Fig 5C and 5D) and were faster than those of acquired with AV for both dye-labeled probes. For instance, BFl and BcO at 25˚C, presented k_{on} values when binding to SAV that were 4X and 3.2X faster than those observed when binding to AV, respectively. However, the temperature dependence was weaker than that observed for AV which indicated a profound difference in the binding site properties of these two proteins, as reveled by an Arrhenius plot (see 3.9 Thermodynamic Parameters). Thus, SAV should be a more robust system for purification applications as variations on the temperature incubation protocols have less negative significant effects in the yield.

Comparisons with other SAV-B_7 association kinetic studies. An independent SF study tracked the binding of unlabeled B_7 by fluorescence quenching of the tryptophan (Trp) of SAV, yielding a k_{on} of $7.5 \pm 0.6 \times 10^{7}$ $M^{-1}s^{-1}$ (at 25˚C and pH 7) [39] which was in excellent agreement with $7.5 \pm 0.2 \times 10^{7}$ $M^{-1}s^{-1}$ for the BFl probe (at 25˚C and pH 8). This finding strongly indicates that the attached dyes are innocuous and dependably monitor the B_7 binding to SAV and presumably to AV. In addition, the absence of any detectable intermediate in the association reaction in both cases is remarkable, since we monitored the initial binding of B_7 and SAV using the fluorescence change and fluorescence anisotropy signals, and the independent tryptophan-quenching experiments observed the final docking of B_7 near the Trp [39]. Conversely, there is another independent Surface Plasma Resonance (SPR) study of immobilized B_7 binding to SAV that yielded a slower k_{on} of 5.1×10^{6} $M^{-1}s^{-1}$ at 4˚C [66], which was ~5X slower than our 2.6×10^{7} $M^{-1}s^{-1}$ at 4˚C, calculated by an Arrhenius plot (ln k_{on} vs 1/T) of the BFl data. Similarly to AV, we believe that the SPR methodology for the B_7 and AV-like protein kinetics [20, 39] was modified by the immobilization of one reactant, either B_7 or protein, to the chip.

Biotinylated and dye-labeled DNA duplex association reaction to AV and SAV

Association rate constants of B_7 attached to biotin-DNA_{ds}*Fl. The biotinylated 14-mer duplex association kinetics showed a biphasic behavior with two temperature and concentration dependent rate constants (Table 2, Fig 7) when reacting with both AV and SAV. The

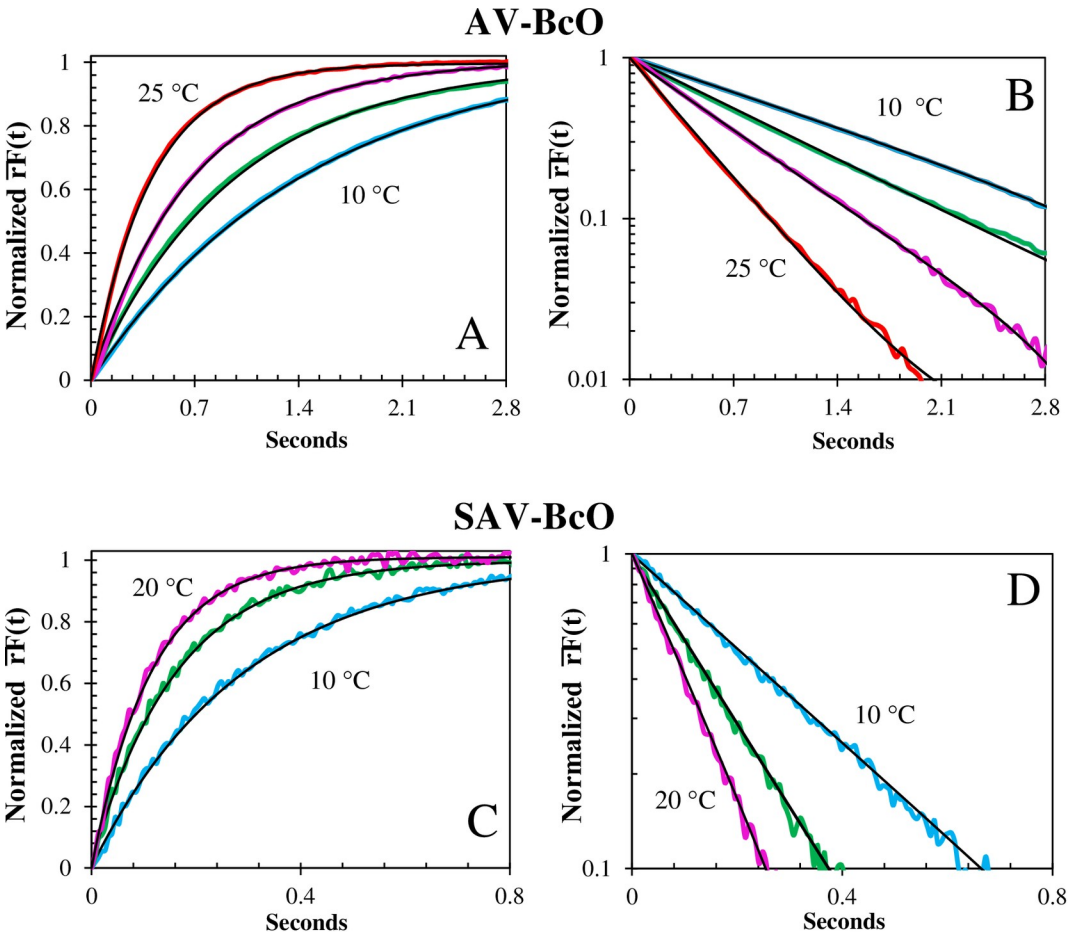

Fig 4. Temperature dependence of the association traces of BcO binding to AV and SAV. (A) Normalized fluorescence anisotropy, $\overline{rF}(t)$, temperature dependence of BcO (20 nM) binding to AV (260 nM) at pH 8, normalized as $[rF(0) - rF(t)]/[rF(0) - rF(\infty)]$. The observed (color) and fitted (black line) curves at 25˚C (top), 20˚C (upper middle) and 15˚C (lower middle) and 10˚C (bottom) had half-times of 280 ms, 452 ms, 695 ms and 1024 ms, respectively; and **(B)** shows the corresponding semi-logarithmic plot of $\overline{rF}(t)$. **(C)** Normalized fluorescence anisotropy, $\overline{rF}(t)$, shows a temperature dependence of BcO (20 nM) binding to SAV (200 nM) at pH 8, normalized as above (4A). The observed (color) and fitted (black line) curves at 20˚C (top), 15˚C (middle) and 10˚C (bottom) had half-times of 79 ms, 111 ms and 202 ms, respectively and **(D)** shows the corresponding semi-logarithmic plot of the $\overline{rF}(t)$.

https://doi.org/10.1371/journal.pone.0204194.g004

biphasic association rate constants, k_{on1} and k_{on2}, summed to approximately 70% of the total reaction amplitude. The remaining ~30% was assigned to a third-rate constant (0.02 ± 0.01 s^{-1}) that presented neither temperature nor concentration dependence; therefore, it has been assigned to the readjustments of the Fl dye after being displaced by both proteins. The k_{on1} and k_{on2} association rate constants of SAV were 3.4X and 1.8X faster than the corresponding rate constants of AV (Fig 8) as observed with the BFl and BcO probes, confirming the differences in the AV and SAV binding pockets.

Comparisons with other biotinylated DNA kinetic studies. An independent FRET study monitored the reaction of B_7 attached to the 5' end of a 46 nucleotide duplex DNA binding to SAV [38]. The reaction also showed two rate constants at pH 8, but at unspecified temperature, pre-exponentials and errors. To make a comparison, we have chosen SAV data at 20˚C whose association rate constant, k_{on1}, of $4.6 \pm 0.8 \times 10^7$ $M^{-1}s^{-1}$ was in excellent agreement with the 4.5×10^7 $M^{-1}s^{-1}$ reported by the mentioned study. In the case of our k_{on2} of

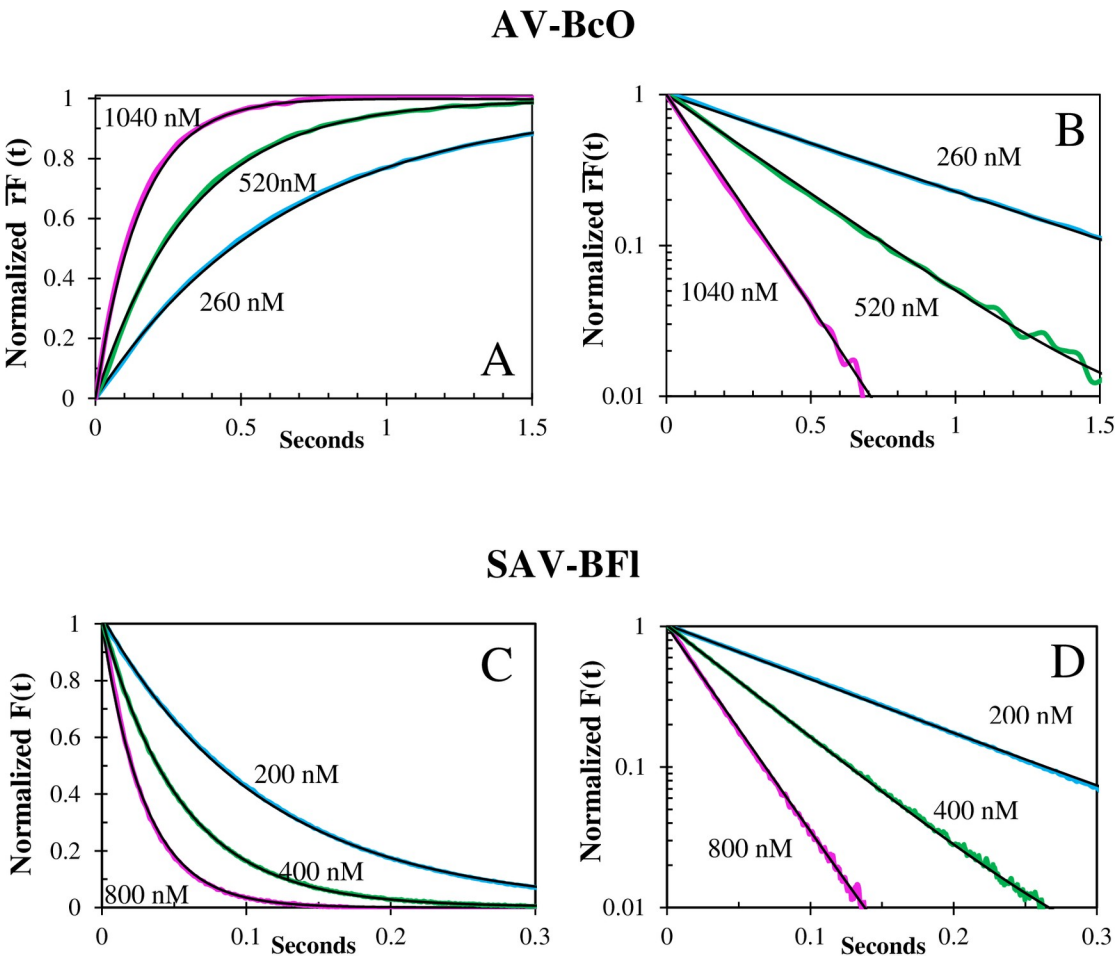

Fig 5. Concentration dependence of association traces of BcO binding to AV and BFl binding to SAV. (A) Corrected Fluorescence Anisotropy Concentration dependence of BcO (20 nM) binding to AV at pH 8 and 20˚C, normalized as $\overline{rF}(t) = [rF(0) - rF(t)]/[rF(0) - rF(\infty)]$. The observed (color) curves were obtained with an AV concentration of 1040 nM (top), 520 nM (middle) and 260 nM (bottom) and the fitted curves (black lines) had halftimes of 109 ms, 229 ms and 455 ms; respectively. **(B)** Shows the corresponding semi-logarithmic plots of $\overline{rF}(t)$. **(C)** Normalized fluorescence change, $\overline{F}(t)$, concentration dependence of BFl (20 nM) binding to SAV at pH 8 and 20˚C. Normalized as followed: $\overline{F}(t) = \frac{F(t)}{F(0)} = [F(t) - rF(\infty)]/[rF(0) - rF(\infty)]$. The observed (color) curves were acquired with SAV concentrations of 200 nM (red), 400 nM (purple) and 800 nM (orange) where the fitted curves (black lines) had halftimes of 77.3 ms, 37.7 ms and 20.6 ms; respectively. **(D)** Shows the corresponding semi-logarithmic plot of $\overline{F}(t)$.

https://doi.org/10.1371/journal.pone.0204194.g005

$2.3 \pm 0.1 \times 10^6$ $M^{-1}s^{-1}$, it was in good agreement with the second rate of 3.0×10^6 $M^{-1}s^{-1}$ of that independent study. The agreement in the data validates our findings which imply that B_7 attached internally to DNA (or at the 5' end) will have two rate constants, one enhanced and other diminished probably due to unfavorable orientation according to the reaction models discussed below.

Significance of the association rate constants

The B_7 binding to AV and SAV (at 25˚C) were, respectively, between 54-714X and 13-400X slower than 10^9 $M^{-1}s^{-1}$ as expected for a diffusion limited process [67]. On the other hand, the k_{on} values of SAV were 3-4X faster than AV's despite the similarity of the AV and SAV binding sites in the crystal structures (Fig 8). Our deglycosylation experiments indicate that the

Table 2. Temperature dependent association rate constants (k_{on}) and thermodynamic values of the dye-labeled B_7 binding to AV and SAV.

Complex[a]	25˚C ($\times 10^{-6} M^{-1}s^{-1}$)	20˚C ($\times 10^{-6} M^{-1}s^{-1}$)	15˚C ($\times 10^{-6} M^{-1}s^{-1}$)	10˚C ($\times 10^{-6} M^{-1}s^{-1}$)	$E_a^{Forward}$ (kcal/mol)	$\Delta S^{\ddagger}$ (cal/˚K·mol)	$\Delta G^{\ddagger}$ (kcal/mol)
AV-BFl	18.5 ± 2.0	10.7 ± 1.6	7.6 ± 2.0	4.86 ± 0.6	14.6 ± 0.6	34.9 ± 2.0	4.2 ± 0.5
AV-BcO (pH 8)[b]	9.5 ± 0.4	5.9 ± 0.4	3.9 ± 0.3	2.6 ± 0.3	14.4 ± 0.6	33.0 ± 2.5	4.6 ± 0.3
AV-BcO (pH 9)	7.9 ± 0.3 [c]	5.4 ± 0.2	3.4 ± 0.1	2.3 ± 0.1	13.9 ± 0.7	30.9 ± 2.5	4.7 ± 0.1
AV-BcO (pH 10)	7.2 ± 0.3 [c]	4.8 ± 0.2	3.0 ± 0.1	1.9 ± 0.1	14.9 ± 0.7	34.1 ± 1.3	4.7 ± 0.3
1) AV-B_7 -DNAds*Fl	15.7 ± 1.0 (30.5%) [d]	11.2 ± 0.8 (68.9%)	7.4 ± 0.7 (87.5%)	4.2 ± 0.5 (95.0%)	14.6 ± 0.8	34.8 ± 3.0	4.2 ± 0.2
2) AV- B_7 -DNAds*Fl	1.4 ± 0.1 (69.5%)	0.98 ± 0.05 (31.1%)	0.70 ± 0.03 (12.5%)	0.52 ± 0.01 (0.05%)	14.2 ± 0.5	29.0 ± 0.5	5.6 ± 0.6
Average	NA	NA	NA	NA	14.4 ± 0.2	32.8 ± 1.2	4.7 ± 0.3
SAV-BFl	74.7 ± 2.0	58.6 ± 1.6	53.1 ± 2.0	45.4 ± 1.0	5.3 ± 0.3	6.6 ± 0.5	3.3 ± 0.6
SAV-BcO	30.3 ± 2.0	24.0 ± 1.6	20.0 ± 1.2	17.3 ± 0.6	6.2 ± 0.4	7.8 ± 0.4	3.9 ± 0.4
1) SAV- B_7 -DNA_{ds}*Fl	53.0 ± 1.0 (44.4%)	45.9 ± 0.8 (50%)	36.4 ± 0.7 (51%)	31.0 ± 0.5 (49%)	6.2 ± 0.4	8.8 ± 0.6	3.5 ± 0.5
2) SAV- B_7 -DNA_{ds}*Fl	2.5 ± 0.1 (55.6%)	2.3 ± 0.1 (50%)	1.7 ± 0.1 (49%)	1.50 ± 0.05 (51%)	6.2 ± 0.5	3.1 ± 0.3	5.3 ± 0.6
Average	NA	NA	NA	NA	6.0 ± 0.2	6.6 ± 1.6	4.0 ± 0.6

The forward thermodynamic values ($E_a^{Forward}$, $\Delta S^{\ddagger, Forward}$ and $\Delta G^{\ddagger, Forward}$) were acquired from global fitting of the rate constants [42, 45] for the most probable model which resulted in a simple reaction with a transition state without intermediates. In the case of the B_7-DNA duplex, the reaction model was a two-serial reaction model also with one transition state without intermediates. The nature of the serial reaction is probably caused by two B_7 populations with different spatial orientations.

[a]The probes were BFl, BcO, and B_7 attached to a nucleotide in a 14-mer DNA duplex and the respective complex with AV and SAV.

[b]The k_{on} values were averaged from data in Table 1

[c]Calculated from an Arrhenius plot.

[d]The pre-exponentials (in parenthesis) of k_{on1} and k_{on2} were renormalized after removing a third process associated with remaining photobleaching.

https://doi.org/10.1371/journal.pone.0204194.t002

disparity in the k_{on} values between both SAV and AV proteins cannot be explained by the presence or absence of the carbohydrate motif on the AV but can be explained by the intermolecular interactions of the aminoacids in the binding pocket and the B_7 ring.

Association reactions of biotin vs. biocytin to SAV and AV

In our study, the association rates were acquired with B_7 and Bc probes, BFl and BcO; respectively, in which Biocytin presents a longer carbon linker. Interestingly, these k_{on} values only differed by 2-fold (Table 1), from 10˚C to 25˚C, when reacting with AV. It is important to clarify that the association rates were not enhanced by the electrostatic attraction of the negative charged probes (BFl and BcO) and the positive AV [32]; since, the association rates of those two probes binding to neutral SAV differed also by ~2 fold as observed for AV. The dissociation constants, K_D, of AV-B_7 and AV-Bc were reported to be 10^{-13} and 10^{-15} M, respectively, differing by 100-fold [40]. Consequently, this 100-fold difference, if accurate, must be caused by a difference of 50-fold in the k_{off}, dissociation rate constants which is discussed below.

Dissociation kinetics

The dissociation reactions of the AV-B_7 and SAV-B_7 complexes have been described as passive unimolecular "replacements" ($k_{off}^{replacement}$) with units of reciprocal seconds (s^{-1}) and values of 9×10^{-8} s^{-1} [35] and 2.4×10^{-6} s^{-1} [68], respectively. However, we have also observed bimolecular "displacement" off-rate constants ($k_{off}^{displacement}$) with $M^{-1}s^{-1}$ units for the SAV-BcO

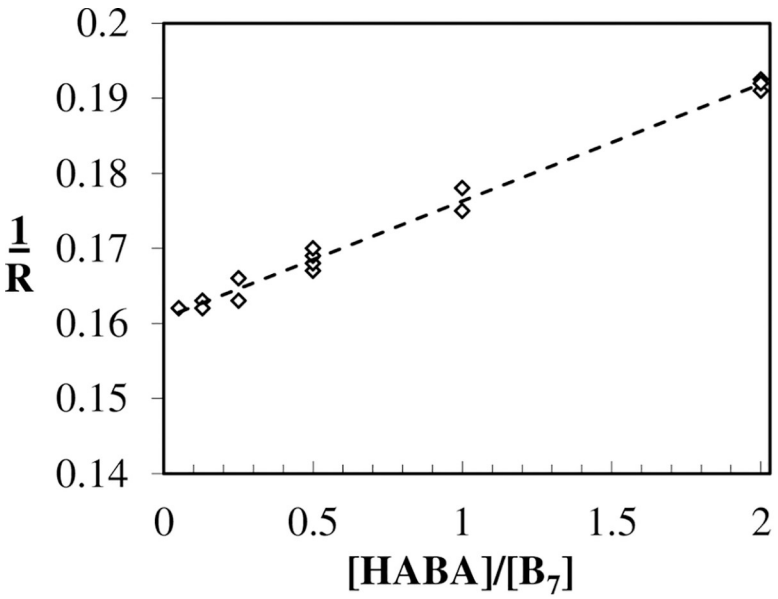

Fig 6. Relaxation kinetics of the AV-HABA complex and unlabeled biotin. The [HABA]/[B_7] is the concentration ratio of these two ligands and the relaxation rate is in s^{-1} (Eq 3). The data points were fitted to a linear regression model yielding a slope and intercept of 0.0156 ± 0.0012 and 0.161 ± 0.005, respectively, resulting in a k_{on}^{B} of 5.3 ± 0.9 × 10^6 $M^{-1}s^{-1}$ at 23˚C. The additional values required for this calculation were HABA association constant to the 4th site when three HABA molecules are already bound: $k_1^{AV-HABA3}$ = 5.1 ± 0.1 × 10^5 $M^{-1}s^{-1}$ and the HABA dissociation of saturated AV-$HABA_4$ complex: $k_{-1}^{AV-HABA4}$ = 6.23 ± 0.11 s^{-1}. The corresponding K_D $^{AV\text{-}HABA}$ = 12.2 ± 0.3 × 10^{-6} M and is in excellent agreement with the 12 × 10^{-6} M reported by Green [60] at pH 8.

https://doi.org/10.1371/journal.pone.0204194.g006

complexes (AB_1 and AB_4) that were strongly dependent on B_7 concentration (Fig 9A) and temperature (Fig 9B). These reactions had ~79% of the total release amplitude, in contrast to the 5% when BFl was used (Fig 9C); therefore, the longer "tail" of the BcO facilitated the displacement for SAV-BcO; and in the case of the SAV-BFl, the electrostatic interactions between negative charged Fl and positive charge SAV prevented the displacement, as observed elsewhere [69]. Thus, longer linkers and neutral dye molecules and proteins are features that can be exploited to increase purification yields. This new information can find important applications in affinity chromatography purification based on SAV and longer "tail" or tethers that will help to increase the release of the product and enhance efficiency. On the contrary, we could not detect neither displacement nor replacement in AV-BFl and AV-BcO complexes since the reaction is very slow (S3 Fig). Thus, in 1966, Green N. determined heroically the $k_{off}^{replacement}$ for AV-B7 in 9 × 10^{-8} s^{-1} for a half-life of 90 days [35] which could not be detected by us since our fluorescence anisotropy methodology is not suitable.

Biotin reaction models of AV and SAV

Reaction model of BFl and BcO binding to AV and SAV. The SF traces of B_7 binding to AV and SAV were best fitted by a simple association model, A + B ⇌ C. A single rate constant, k_{on} (Eq 8), could be fit with no intermediates or evidence of cooperativity considering that the dissociation reaction was not significant for the first 5–8 sec after mixing. More elaborate mechanisms have been reported [70, 71]. For example, A + B ⇌ C ⇌ D has been proposed for polystyrene SAV coated particles (6.5 nM) reacting with a fluorescein labeled B_7 probe (1.8 nM and 17.5 nM), whose linker resembles our BcO probe. This model required fitting of two dissociation and two association rate constants with the extra equilibrium attributed to two

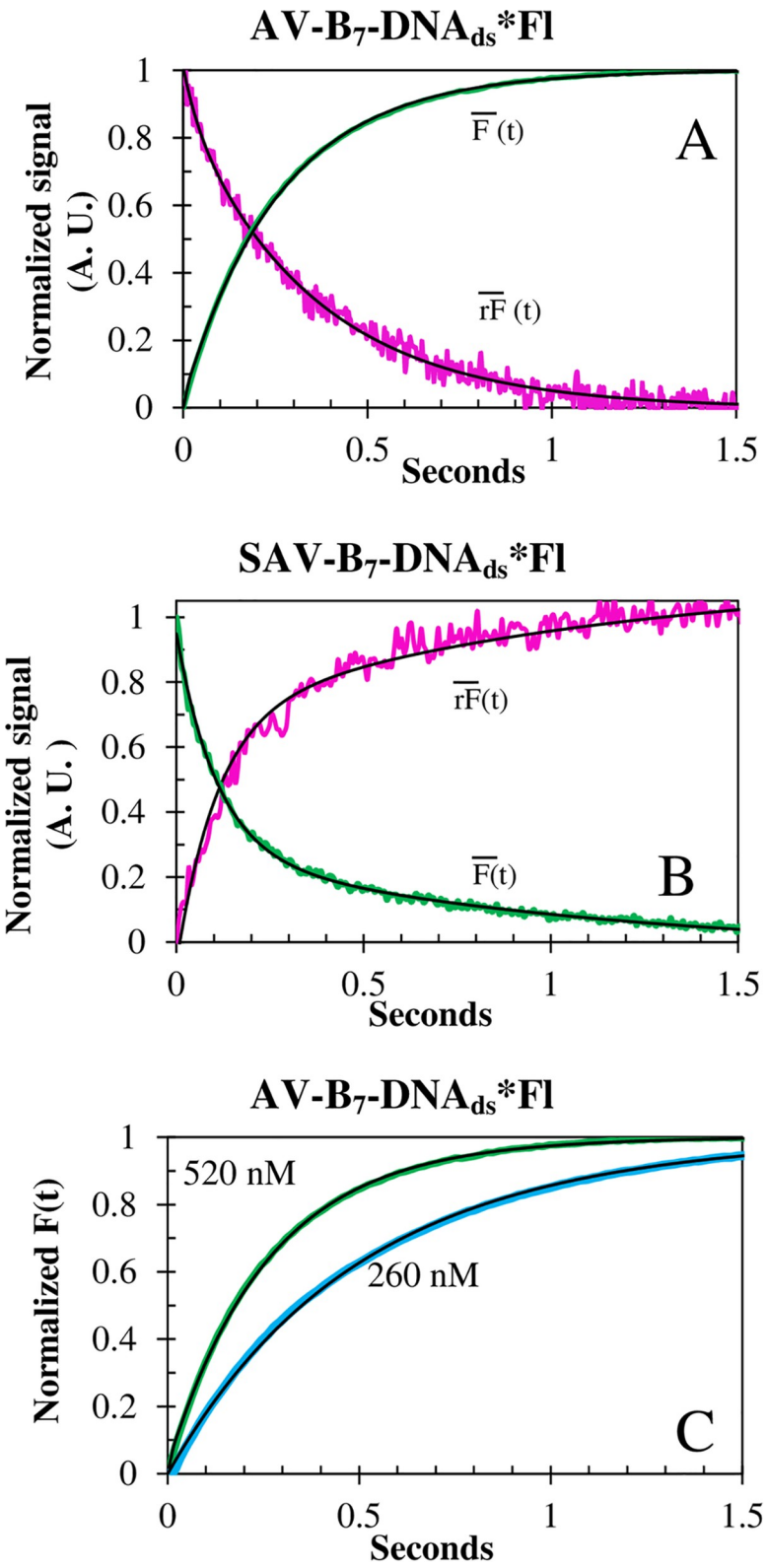

Fig 7. Association traces of biotin-DNA_{ds}*Fl binding to SAV and AV. The $\overline{rF}(t)$ and $\overline{F}(t)$ signals of the association reactions of B_7-DNA_{ds}*Fl (20nM) to **(A)** AV (520 nM) and **(B)** SAV (200 nM), at 15˚C. **(C)** Concentration dependence of B_7-DNA_{ds}*Fl (20 nM) binding to AV at 15˚C. All curves (black line) were strongly biphasic. Notice the inversion of SF signals. However, the $\overline{F}(t)$ traces were in prefect agreement with QY experiments (Table 4).

https://doi.org/10.1371/journal.pone.0204194.g007

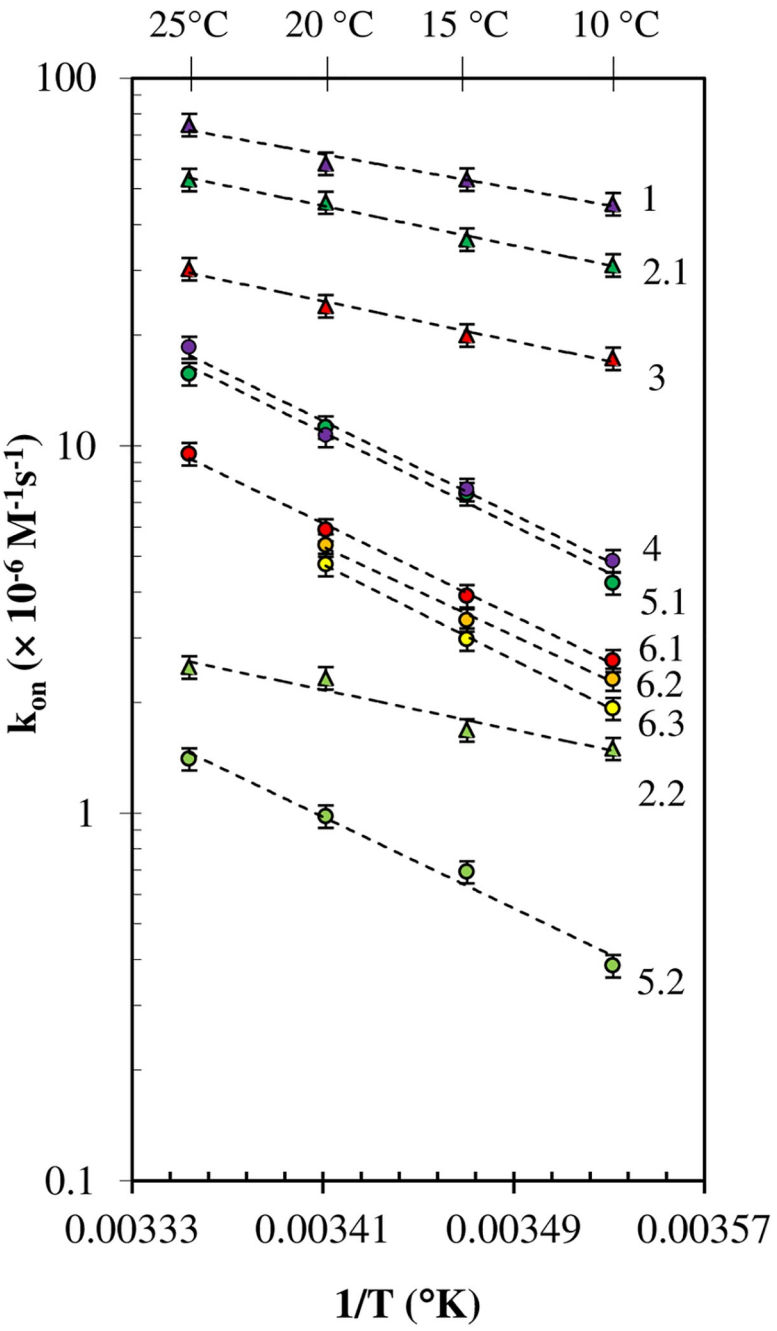

Fig 8. Arrhenius plot of the association rate constants. Temperature dependence of the B_7 association reaction at pH 8 (unless otherwise specified) for: 1 SAV-BFl (purple triangles); 2 SAV-B_7-DNA_{ds}*Fl (green triangles): 2.1 (k_{on1}) and 2.2 (k_{on2}); 3 SAV-BcO (red triangles); 4 AV-BFl (purple circles); 5 AV-B_7-DNA_{ds}*Fl (green circles): 5.1 (k_{on1}) and 5.2 (k_{on2}); 6 AV-BcO (red circles): 6.1 at pH 8, 6.2 at pH 9 (orange circles), 6.3 at pH 10 (yellow circles). The data points were plotted in semi-logarithm (ln k_{on} vs 1/T) for clarity.

https://doi.org/10.1371/journal.pone.0204194.g008

reasons: 1) The interference of the dye structures into the neighboring site due to multiple occupancies on the tetramer [61] and 2) to possible inhibitory steric interactions caused by high density of SAV sites on the surface of the polystyrene particles. Interestingly, a similar model was used to analyze a pull-off study carried out by Scanning Force Microscopy for

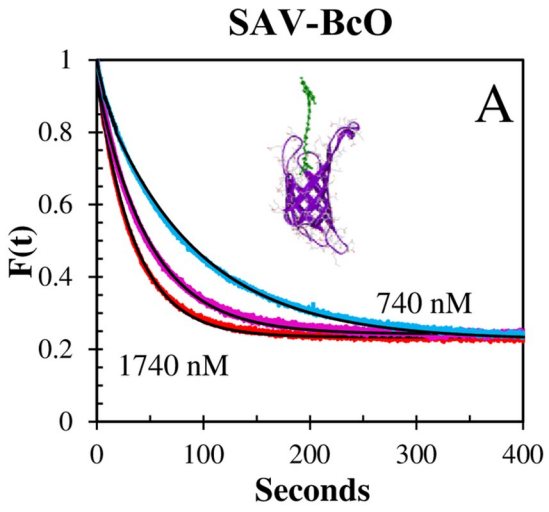
SAV-BcO
A
740 nM
1740 nM
F(t)
Seconds
0
0.2
0.4
0.6
0.8
1
0
100
200
300
400

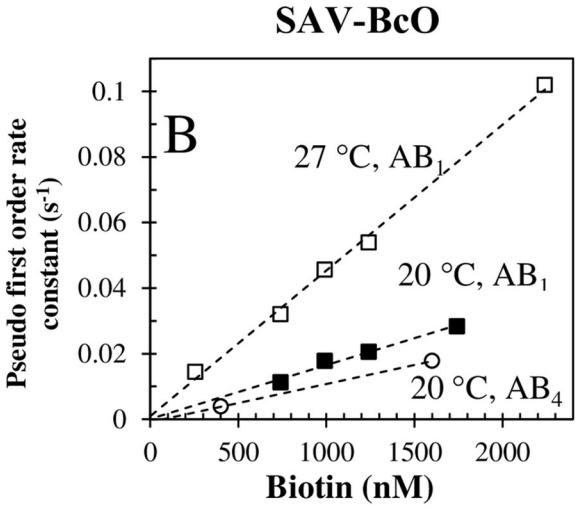
SAV-BcO
B
27 °C, AB1
20 °C, AB1
20 °C, AB4
Pseudo first order rate constant (s-1)
Biotin (nM)
0
0.02
0.04
0.06
0.08
0.1
0
500
1000
1500
2000

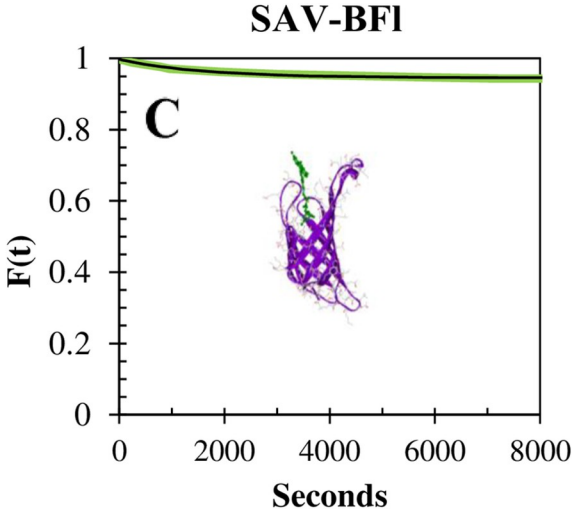
SAV-BFl
C
F(t)
Seconds
0
0.2
0.4
0.6
0.8
1
0
2000
4000
6000
8000

Fig 9. Dissociation kinetics of SAV-BcO and SAV-BFl complexes. (A) Concentration dependence of the displacement reaction of SAV-BcO complex (AB_1 model) by unlabeled B_7 at 20˚C. The concentration of challenging B_7 was 740 nM (blue), 1240 nM (pink) and 1740 nM (red) after the remaining free binding sites were filled. The half-times were 56.6 s, 33.9 s and 24.2 s, respectively; with a release amplitude of 79 ± 1%. **(B)** Temperature dependence of the displacement reaction of SAV-BcO by unlabeled B_7 for the AB_1 filling model (at 20˚C and 27˚C) and for the AB_4 model (at 20˚C). The corresponding $k_{off}^{displacement}$ (calculated from the slope) were $1.6 \pm 0.4 \times 10^5$ $M^{-1}s^{-1}$, $4.6 \pm 0.3 \times 10^5$ $M^{-1}s^{-1}$ and $1.2 \pm 0.3 \times 10^5$ $M^{-1}s^{-1}$, respective. **(C)** Displacement reaction of unlabeled B_7 and SAV-BFl complex (AB_1 filling model) at 30˚C. The concentration of challenging B_7 was 1400 nM which produced a release of only 5% of the bound probe. The green curve is the observed data and black curve is the fitted curve for which only 6.5% displacement was observed for SAV-BFl complex in contrast with 79% in case of the complex formed with the longer linker BcO.

https://doi.org/10.1371/journal.pone.0204194.g009

AV-B complex with immobilized AV in which two events of 20–40 pico-newtons and 40–80 pico-newtons were assigned to the presence of an intermediate [72]. Categorically, we have avoided these experimental complications by following the reaction at pseudo first order to ensure that our probes occupied only one binding site of AV and SAV in solution (non-immobilized), as discussed above. However, when considering a particular AV or SAV bioassay, one must consider that the surface matrix complexity, the multiple orientations of B_7, and the modifications of the AV-like proteins can modify the dissociation mechanism with respect to those observed in solution by us.

Reaction model of biotin-DNA_{ds}*Fl binding to AV and SAV. The B_7 binding kinetics, when attached to DNA, was best described by two parallel reactions (Eq 9) with two independent association rate constants that showed no evidence of intermediates in solution. The pre-exponentials of the rate constants were temperature dependent (Table 2) suggesting the presence of two B_7 populations with different orientations with respect to the DNA and responsible for the measured k_{on1} and k_{on2} rate constants. Thus, at 25˚C, the measured values of k_{on1} for both AV and SAV were only 20–40% slower than rate constants acquired with BFl, which suggests that B_7 on the DNA was positioned in a favorable orientation that enhances the association reaction. On the other hand, the slower k_{on2} rate constant is associated with an unfavorable orientation of the second B_7 population which could be partially intercalated in the stacked nucleotides.

Thermodynamic parameters

The forward activation energies ($E_a^{forward}$ or $\Delta H^{\ddagger,forward}$) of the B_7 binding to AV and SAV were ~6.0 and ~14 kcal/mol, respectively; and they were in good agreement with early estimations of 10–12 kcal/mol for the displacement of water molecules from the binding pocket [60]. These values were larger than the 3–4 kcal/mol [35, 73] characteristic of a diffusion limited reaction (which requires also association rate constants in the order of 10^9 $M^{-1}s^{-1}$ while our fastest values were in the order of ~1.9×10^7 $M^{-1}s^{-1}$ and ~7.5×10^7 $M^{-1}s^{-1}$, at 25˚C for AV-BFl and SAV-BFl, respectively). Hence, the association reaction is not diffusion controlled in the range of experimental work carried by us. Interestingly, the B_7 binding process for both proteins share the same k_{on} at 52.1˚C (calculated by Arrhenius plot), and binding of B_7 ligand enhances thermal stability of the proteins shifting from 75˚C to 112˚C for SAV and from 84˚C to 117˚C for AV [74].

Remarkably, the difference of forward and reverse activation energies ($E_a^{forward}$—$E_a^{backward}$), calculated with Arrhenius plots of the association and dissociation rate constants, respectively; matched, within the error, the reaction enthalpy (ΔH°_{Rxn}) calculated by calorimetry (Table 3, Fig 10A). The same argument holds for the Gibbs free energy ($\Delta G^{\ddagger,\ forward}$-$\Delta G^{\ddagger,\ backwards}$) and entropy ($\Delta S^{\ddagger,\ forward}$-$\Delta S^{\ddagger,\ backwards}$), and the calorimetric ΔG°_{Rxn} and ΔS°_{Rxn} values have been

Table 3. Thermodynamic cycles of B_7 binding to AV and SAV for one transition state.

1) Complex	2) ΔH°_{rxn} [a] (kcal/mol)	3) $E_a^{Forward}$, b (kcal/mol)	4) $E_a^{Backward}$, a (kcal/mol)	5) $\Delta E = E_a^{Forward} - E_a^{Backward}$ (kcal/mol)[c] column 3 minus 4
AV-B_7	-20.3 ± 0.3 [76] -22.5 ± 0.1 [77] -26.7 [39] -23.4 ± 0.3 [78] -23.2 ± 1.7[d]	14.4 ± 0.2	37.6 ± 2.0 [18]	-23.2 ± 2.2
SAV-B_7	-23.0 [79] -24.5 [39] -24.9 ± 0.4 [80] -26.7 [19] -24.8 ± 2.0	6.0 ± 0.2	32.0 [81] 30.4 ± 0.2 [39, 80] 25.8 ± 1.2 [82] 29.4 ± 2.6	-23.4 ± 4.0
1) Complex	**2) ΔS°_{rxn} (cal/mol°K)**	**3) $\Delta S^{\circ\,\ddagger,\,Forward}$ (cal/mol°K)**	**4) $\Delta S^{\circ\,\ddagger,\,Backward}$ (cal/mol°K)**	**5) $\Delta S^{\circ\,\ddagger,\,Forward} - \Delta S^{\circ\,\ddagger,\,Backward}$ (cal/mol°K), column 3 minus 4**
AV-B_7	-8.9 [78]	32.0 ± 1.2	43.0 ± 2.0 [18][e]	-11.0 ± 2.5
SAV-B_7	-21.0 [39]	6.7 ± 1.6	29.9 ± 2.0 [18][e] 25.8 [81] 18.8 ± 0.3 [39, 80, 82] 24.8 ± 4.5	-18.1 ± 4.5
1) Complex	**2) ΔG°_{rxn} (kcal/mol)**	**3) $\Delta G^{\circ\,\ddagger,\,Forward}$ (kcal/mol)**	**4) $\Delta G^{\circ\,\ddagger,\,Backward}$ (kcal/mol)**	**5) $\Delta G^{\circ\,\ddagger,\,Forward} - \Delta G^{\circ\,\ddagger,\,Backward}$ (kcal/mol) column 3 minus 4**
AV-B_7	-20.5 [76] -20.8 [78] -20.7 ± 0.3	4.7 ± 0.3	24.7 ± 2.0 [18][e]	-20.0 ± 4.0
SAV-B_7	-18.1 [39] -18.3 [83, 84] -18.2 ± 0.2	4.0 ± 0.6	21.4 ± 2.0 [47] 24.8 ± 0.3 [80][f] 24.6 ± 0.3 [39, 82] 23.6 ± 1.5	-19.6 ± 2.5

Experimental forward parameters ($E_a^{Forward}$, $\Delta S^{\circ\,\ddagger,\,Forward}$ and $\Delta G^{\circ\,\ddagger,\,Forward}$, in column 3) calculated by us, are in a good agreement with the experimental calorimetry values (ΔH°_{rxn}, ΔS°rxn and ΔG°rxn, in column 2) and dissociation parameters ($E_a^{Backward}$, $\Delta S^{\circ\,\ddagger,\,Backward}$ and $\Delta G^{\circ\,\ddagger,\,Backward}$, in column 4) when a one-transition state reaction model is considered.

[a]Column 2 and 4 contain data obtained in previous studies. Comparisons between reported values are made, and the average value is placed below the dotted line.

[b]The forward and reverse rate constants were used to calculate, with Arrhenius plots, the respective forward and backward activation energies, $E_a^{forward}$ and $E_a^{backwards}$, respectively

[c]Column 5 is column 3 minus column 4 and should be equivalent to experimental reaction values obtained from multiple studies thus confirming the accuracy of the proposed model. The difference of these activation energies results in ΔE (column 5) which were equivalent to an averaged ΔH°_{Rxn} (column 1) of multiple independent calorimetry studies. Similarly, analysis was carried out for reaction Gibbs free energy (ΔG°_{Rxn}) and entropy (ΔS°_{Rxn}).

[d]Averaged values are shown below the dotted line.

[e]Calculated from the plotted data.

[f]Calculated at 25°C.

https://doi.org/10.1371/journal.pone.0204194.t003

calculated by others (see references in Table 3, Fig 10B and 10C); Thus, the forward thermodynamic parameters obtained in this study completed nicely the thermodynamics cycles, thus making very compelling arguments in favor of the proposed simple reaction model (Eq 8), which has a single transition state (‡) but no intermediate. The positive nature of $\Delta E_a^{forward}$ and $\Delta S^{\ddagger,\,forward}$ toward the transition state can be explained as the energy required to remove water molecules and displace the protein's β3-β4 loop [32, 75] with an increment of the overall

Table 4. Spectroscopic parameters of the dye-labeled B_7 probes and respective complexes with AV and SAV.

Sample [a]	Maximum Absorbance (nm)	Maximum Emission (nm)	Lifetime τ [b]	Natural Lifetime τ° [c]	Dynamic Quantum Yield Φ [d]	Quantum Yield QY	Fraction of Non-Statically Quenched Dye 1-S [e]	Steady State Anisotropy r_{ss} [f]	Cone Angle Ω [g]
BFl	494	530	4.03 ± 0.01	5.2 ± 0.2	0.81 ± 0.04	0.52 ± 0.02	0.65 ± 0.06	0.021 ± 0.002	90
AV-BFl	498	528	4.22 ± 0.01	4.7 ± 0.1	0.90 ± 0.02	0.44 ± 0.01	0.49 ± 0.03	0.180 ± 0.003	51 ± 2
SAV-BFl [h] mono-ionic	472	515	3.0 ± 0.1	8.1 ± 0.1	-	0.06 ± 0.01 [i]	0.18 ± 0.02	0.171 ± 0.008	51 ± 2
SAV-BFl di-ionic	494	528	4.1 ± 0.1	4.5 ± 0.1	-		0.49 ± 0.03		
BcO	495	523	3.75 ± 0.04	4.4 ± 0.1	0.85 ± 0.02	0.91 ± 0.02	1.00 ± 0.02	0.023 ± 0.002	90
AV-BcO	497	524	4.35 ± 0.01	4.9 ± 0.1	0.88 ± 0.02	0.62 ± 0.02	0.70 ± 0.03	0.187 ± 0.009	50 ± 2
SAV-BcO	497	524	3.98 ± 0.01	4.8 ± 0.1	0.83 ± 0.02	0.21 ± 0.01	0.25 ± 0.02	0.053 ± 0.005	50 ± 2
B_7-DNA_{ds}*Fl	502	520	3.12 ± 0.08	4.3 ± 0.1	0.75 ± 0.04	0.22 ± 0.01	0.29 ± 0.02	0.077 ± 0.005	49 ± 2
AV-B_7 -DNA_{ds}*Fl	499	521	3.80 ± 0.05	3.9 ± 0.1	0.98 ± 0.02	0.36 ± 0.01	0.37 ± 0.02	0.150 ± 0.007	40 ± 3
SAV-B_7 -DNA_{ds}*Fl	499	521	3.86 ± 0.01	3.9 ± 0.1	1.00 ± 0.02	0.18 ± 0.01	0.18 ± 0.02	0.082 ± 0.001	51 ± 3

The chemical environment is altered after complex formation as changes in the following properties shown: shifting in absorbance peaks (abs max, S1 Fig) and fluorescence emission peaks (emi max, S2 Fig), lifetimes (τ), dynamic quenching (Φ), static quantum yields (QY), fluorescence emitting population (1-S) and the cone angle that indicates dye mobility (Ω).

[a]Experiments were carried out with protein excess (AB_1 filling model).

[b]Bi-exponential decays were observed for the B_7-DNA_{ds}*Fl and SAV-BFl complexes (S1 Table).

[c]τ°, is the intrinsic lifetime of the fluorescent dye when there are no other radiationless transitions.

[d] $\Phi = \Sigma\alpha\tau/\tau^\circ$, is the dynamic quantum yield.

[e]1-S = QY/Φ, is the fraction of non-statically quenched dye.

[f]r_{ss}, is the steady state anisotropy measured at 20˚C.

[g]Ω, is the cone angle measured in degrees at 20˚C

[h]The absorbance spectrum of the SAV-BFl complex (S1 Fig) and the detection of the corresponding lifetimes of 3.0 and 4.1 ns [85, 86] indicates the presence of both Fl^{1-} and Fl^{2-}, respectively [79]. We used these reported lifetimes to calculate the pre-exponentials values (α) of each fluorescent species in the SAV-BFl complex. The intrinsic lifetime of Fl^{1-} was calculated by dividing the lifetime (3.0 ns) over the absolute quantum yield (0.37) [46]. We calculated the $(1\text{-}S)_{Fl}{}^{1-}$ by assuming that $(1\text{-}S)_{Fl}{}^{2-}$ is that of AV-BFl (with contains only Fl^{2-}) and solving the following equation: $\frac{\alpha_{Fl2-}}{\alpha_{Fl1-}} = \frac{[C\ \varepsilon\ (1-S)D]_{Fl2-}}{[C\ \varepsilon\ (1-S)D]_{Fl1-}}$, where C is the concentration, ε is the molar absorptivity at 470 nm, D is the fraction of photons under a band width of 520 nm ± 5 nm of the normalized emission spectrum of Fl^{2-} and Fl^{1-} (taken from Fig 7 [86]) which values were 0.229 and 0.158, respectively. The $\alpha_{Fl}{}^{2-}$ and $\alpha_{Fl}{}^{1-}$ were 0.611 and 0.388, respectively; for a ratio of 1.574. The concentration of Fl^{2-} and Fl^{1-} were acquired by solving simultaneously the following equations: $abs^{494} = (\varepsilon^{494} {}^{*}C)_{Fl}{}^{1-} + (\varepsilon^{494} {}^{*}C)_{Fl}{}^{2-}$ and $abs^{472} = \varepsilon^{472}\ C_{Fl}{}^{1-} + \varepsilon^{472}\ C_{Fl}{}^{2-}$, where *abs* is the absorbance at 494 nm and 472 nm of the SAV-BFl absorbance spectrum; and the ε of Fl^{1-} is 25 $mM^{-1}cm^{-1}$ and 29 $mM^{-1}cm^{-1}$ at 494 nm and 472 nm, respectively; and ε of Fl^{2-} were 76 $mM^{-1}cm^{-1}$ and 35 $mM^{-1}cm^{-1}$ [86, 87] at 494 nm and 472 nm. Thus, for the SAV-BFl complex, the concentration ratio of Fl^{1-}/Fl^{2-} was 3.5.

[i]The QY and Φ of the SAV-BFl complex could not be resolved for each of the two Fl species.

https://doi.org/10.1371/journal.pone.0204194.t004

disorder, $\Delta S^{\ddagger}$. A comparative analysis of the transition state (‡) for the AV-B and SAV-B complexes reveals that the former has a larger $\Delta E_a{}^{forward}$ and $\Delta S^{\ddagger,forward}$ (Table 3, Fig 10, red line) than the latter (Table 3, Fig 10, green line) which implies that binding sites of AV are deeper and less accessible resulting in slower association rate constants and larger activation energy with respect to B_7 binding to SAV.

Fluorescence spectroscopic parameters of labeled probes and complexes

The absorbance and emission peaks of all the dye-labeled B_7 complexes (Table 4) were red shifted a few nanometers (Supporting Information, S1 and S2 Figs) with respect to the

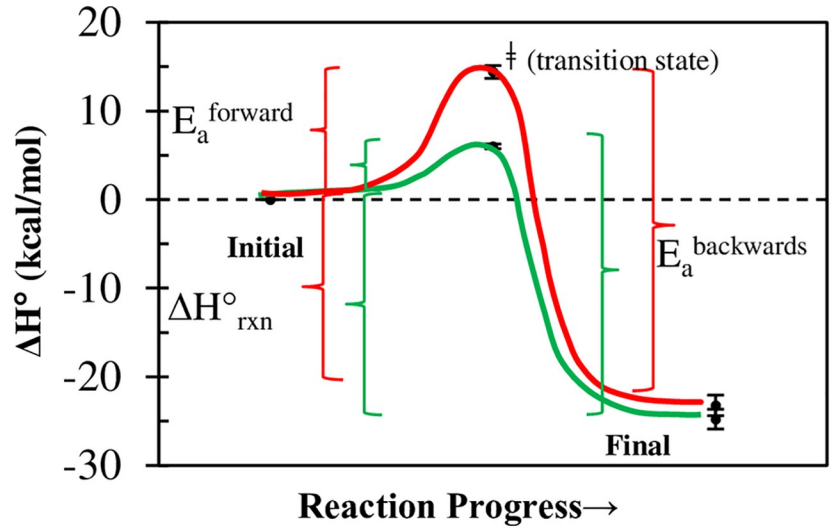
20
10
0
-10
-20
-30
ΔH° (kcal/mol)
‡ (transition state)
E_a forward
Initial
ΔH°_rxn
E_a backwards
Final
Reaction Progress→

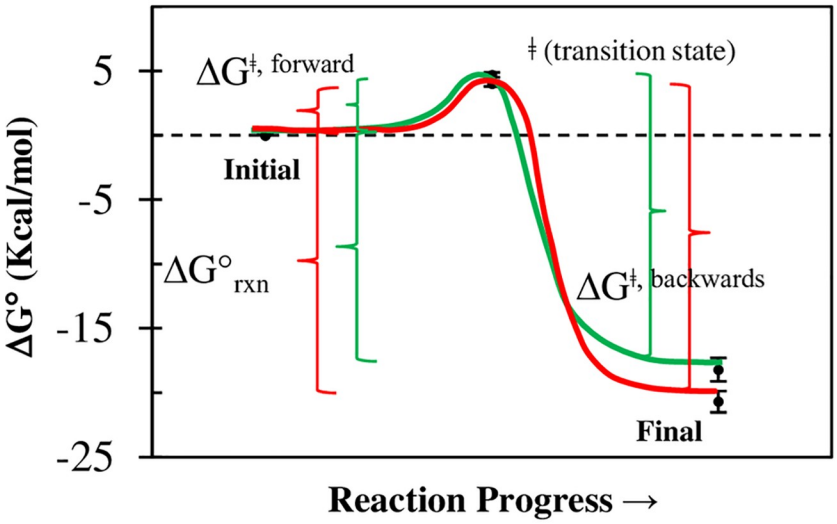
5
-5
-15
-25
ΔG° (Kcal/mol)
ΔG‡, forward
‡ (transition state)
Initial
ΔG°_rxn
ΔG‡, backwards
Final
Reaction Progress →

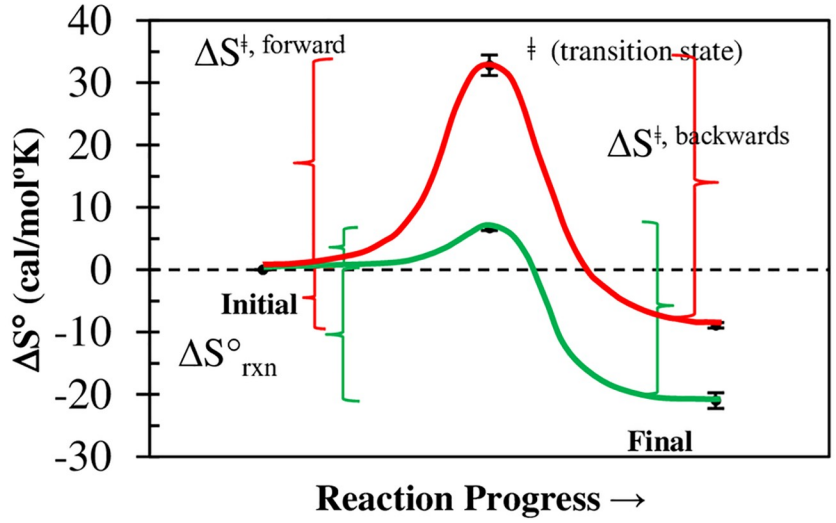
40
30
20
10
0
-10
-20
-30
ΔS° (cal/molºK)
ΔS‡, forward
‡ (transition state)
ΔS‡, backwards
Initial
ΔS°_rxn
Final
Reaction Progress →

Fig 10. Thermodynamic cycle of the B_7 binding to AV and SAV. (**A**) Enthalpy, **(B)** entropy, and **(C)** Gibbs free energy of the B_7 binding to AV (red) and SAV (green) for one transition state and no intermediate. The ΔH°_{rxn}, ΔS°_{rxn}, and ΔG°_{rxn} correspond to the average values found in multiple studies (Table 3). Arrhenius plots of the temperature dependent association and dissociation rate constants were used to calculate the $E_a^{forward}$ and $E_a^{backwards}$, respectively.

https://doi.org/10.1371/journal.pone.0204194.g010

unbound probes, with the exception of the B_7-DNA_{ds}*Fl complexes with AV and SAV that were blue-shifted 3 nm by the presence of both proteins. This can be explained by fluorescein (Fl) interactions with DNA_{ds} before binding to AV and SAV which is later displaced to the solution in the complex. In the particular case of the absorbance spectrum of SAV-BFl, it was highly distorted (S1 Fig) owing to the shifting of the Fl^{-2}/Fl^{-1} equilibrium by charge transfer [79]; since, we detected the corresponding 4.1 ns and 3.0 ns lifetimes (τ). The time-resolved fluorescence of B_7-DNA_{ds}*Fl complexes of SAV and AV proteins (S1 Table) had two lifetimes decays of 0.72 (± 0.01) ns and 3.78 (± 0.01) ns, and 2.29 (± 0.02) ns and 4.08 (± 0.01) ns, respectively; whose exponentials were not affected by temperature suggesting the existence of the two Fl positions on the DNA which make a compelling argument for the parallel reaction model (Eq 9) with two reacting populations: $(Biotin\text{-}DNA_{ds}{}^{*}Fl)_1$ and $(Biotin\text{-}DNA_{ds}{}^{*}Fl)_2$.

The deconvolution of the SF binding traces was completed using the steady-state anisotropy (r_{ss}) whose AV values were larger than SAV attributable to a larger molecular weight and to the presence of the carbohydrate motif for the former. Significantly, the quantum yields (QY) of the complexes were in excellent agreement with all the binding association amplitude changes. Thus, in the case of the B_7-DNA_{ds}*Fl reactions, the traces had shifted directions (Fig 7) since there are opposite quenching interactions when SAV and AV complex are formed. The quantum yield, of the free probe B_7-DNA_{ds}*Fl was QY = 0.22 ± 0.01 (Table 4) incremented up to 0.36 ± 0.01 for the AV-B_7-DNA_{ds}*Fl complex and decreased to 0.18 ± 0.01 for the SAV-B_7-DNA_{ds}*Fl complex. This effect is caused by the bulkier nature of the AV with respect to SAV that allows further displacement of Fl from the 3' end toward the solution environment resulting in the increase of the QY for the B_7-DNA_{ds}*Fl-AV.

The (S) and (1-S) are, respectively, the static and non-statically quenched dye populations. The latter always decrease with the complex formation with respect to the unbound free probes; however, the fluorescence information pertained to the self-revealing population whose cone angles (Ω) of ~50˚ pointed out that the dye probe was fairly free to rotate (Fig 11) in the complexes. On the other hand, the presence of quenching did not affect the accuracy of association rate values, as the rates obtained in the independent SAV tryptophan-quenching study [39] and our data were in perfect agreement.

Conclusions

In the presented study, we calculated the association rate constants of B_7 binding to AV and SAV with dye-labeled B_7 probes and unlabeled B_7. We concluded that attached fluorescent probes did not alter the association rates and no binding cooperativity was observed when comparing the initial (unoccupied) and final (occupied) binding rates. The fluorescence, $\overline{F}(t)$, and corrected anisotropy signals, $\overline{rF}(t)$, of the dye-labeled B_7 probes provided truthful binding traces contrary to the uncorrected anisotropy signal, $\overline{r}(t)$, due to changes in the QY of the participating reacting species. The B_7 association rate constants of SAV are several times faster than AV and the glycan chain of the latter does not play a role in the B_7 binding association and neither explains the difference in the k_{on} values between these two proteins. Thus, we conclude that the main differences in reaction speeds are likely related to the accessibility to the binding pocket in solution, and due to the open form in the shorter loop in SAV (residue 45 to 52, 8 residues) [81] in comparison with the AV's 12-residue loop L2-L3 (residue 35–46) [89].

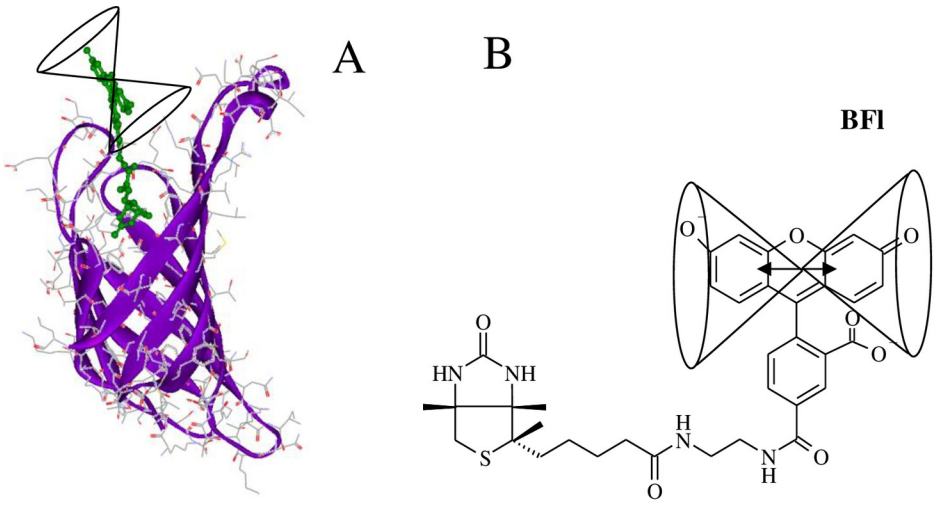

Fig 11. Pictorial representation of the AV-BFl complex. (A) The fluorescein dye in the complex has a relative high dye mobility with a half apical angle [88] (**Ω**) of 51˚ ± 2˚ in contrast with the unrestricted mobility (90˚) of the dye in the unbound BFl. **(B)** The figure reflects rotational motion of the transition moment of the isoalloxanzine ring system within the cone. The dye structure was added using Accelrys DS visualizer 2.0 to the AV-B crystal structure complex: 2AVI [32]. Figures only show one binding site for clarity purposes.

https://doi.org/10.1371/journal.pone.0204194.g011

Also, the variation in requirements for an induced fit could explain larger activation energy and entropic increment for AV compared to the SAV in the overall thermodynamics of the reaction. Interestingly, the overall reaction free energy changes are equivalent.

The association rate constant for BcO, in which the tag is attached to a longer linker of biocytin, is ~2X faster than B_7 with the shorter linker (BFl) for both proteins. The difference of 100X in K_D of AV complex with B_7 and biocytin can be explained by differences in the dissociation process rather than the association rate constants. The B_7 binding to AV and SAV is not diffusion limited as larger than 3 kcal/mol activation energies were calculated with Arrhenius plots of the rate constants, and those rates were two orders of magnitude slower (on average ~10^7 $M^{-1}s^{-1}$) than the 10^9 $M^{-1}s^{-1}$ required for diffusion limited reactions. The forward thermodynamic parameters of B_7 binding to AV and SAV complemented nicely the thermodynamic cycles with data obtained with independent calorimetric studies and dissociation kinetics elsewhere. Thus, the most probable reaction model is the one without a chemical intermediate and a single transition state in solution, but it could be more elaborate on support matrices, such as in chip assays.

The spectroscopic properties indicated very compact complexes with high dye mobility for all the probes, BFl, BcO and B_7-DNA_{ds}*Fl. We report for the first time a bimolecular displacement rate constant value for the SAV-BcO complex when challenged by unlabeled B_7 and this displacement of the B_7 with the longer linker (biocytin) in the BcO; this suggests that the repair and reconditioning of enriched B_7-avidin-like surfaces is possible if long linkers are used. Early observations of affinity variations depending on the linker lengths for similar dye-labeled B_7 probes have been showed in incubation anisotropy titrations [90] but the paper did not systematically study the rate constants at various conditions (Tables 1 and 2) and multiple spectroscopic values (Table 4) of the probes as carried out here.

The AV and SAV complexes are highly thermally stable at 112˚C and 117˚C [74]; respectively, and a possible application of dye-labeled B_7 and AV-like complex could be in Dye- Sensitized Solar Cells (DSSC) [91, 92] as the photon harvesting dye can be displaced when damaged. The protein can be attached covalently to the n-type material (e.g. TiO_2) and the charge-transfer

molecule to B_7 (e.g., porphyrins, chlorophylls, ruthenium-complexes, coumarins or indoline dyes [93]), with the advantage of regeneration capabilities, as damaged dye can be reconditioned or replaced by another dye type on the tetramer attached surface (Fig 9A). This technique could be simpler than switchable mutants of avidin for regenerative biosensors reported elsewhere [94, 95]. The spectroscopic properties of these dye-labeled B_7 and AV-like complexes are vital for detection methods based on polarization, fluorescence, anisotropy and Fluorescence Resonance Energy Transfer (FRET) systems because static, dynamic quenching and rotational constraints of the fluorescent probes reduce the detection limits by decreasing the signal to noise ratios [96] and producing artifacts. The information here presented will be valuable to improve new nano-technological applications of B_7 and AV-like protein systems.

Supporting information

S1 Fig. Absorbance spectra of dye-labeled B_7 probes and respective complexes with AV and SAV. The absorbance spectra of the unbound BFl, BcO and B_7-DNA_{ds}*Fl are shown in dark blue and the respective bound complexes formed with SAV and AV in pink. The spectra are normalized to the calculated molar absorptivies. The distortion of the SAV-BFl absorbance spectrum (B panel) is caused by the presence of Fl^{2-} and Fl^{1-}. The labeled probes and protein concentrations were 1 μM and 10 μM, respectively.
(DOCX)

S2 Fig. Fluorescence emission spectra of dye-labeled B_7 and respective complexes with AV and SAV. The normalized spectra of the unbound BFl, BcO and B_7-DNA_{ds}*Fl are shown in blue and their respective bound complexes formed with SAV and AV in pink. The probe and protein concentrations were 20 nM and 1040 nM (AB_1 filling model), respectively.
(DOCX)

S3 Fig. Dissociation reactions of AV-BcO and AV-BFl complexes by unlabeled B_7 at 20˚C. The dissociation reactions of AV complexes were carried out with a preformed complex of 20 nM BFl or BcO and 260 nM AV for a filling model of AB_1 and challenged with unlabeled B_7 at 2,000 nM. The $k_{off}^{displacement}$ could not be detected and the corresponding $k_{off}^{replacement}$ (9×10^{-8} s^{-1}) found by Green N. [35] is too slow to be determined by the our fluorescence anisotropy methodology.
(DOCX)

S1 Table. Lifetimes of dye-labeled B_7 probes and protein complexes. The fluorescence lifetimes are shown in nanoseconds and were obtained in solution.
(DOCX)

S1 File. Excel file with data values.
(XLSX)

Acknowledgments

Roberto F Delgadillo thanks Dr. Efrain Barragan, Dr. Omar Olmos-Lopez and Ms. Lola R. for their support; Dr. Justin Shearer, Andrea R. Gomez-Fernandez and Dr. Yuriana Oropeza for proof reading the manuscript; CONACYT-Mexico for the postdoctoral and SNI grants; and the Government of Veracruz-Mexico. Roberto F. Delgadillo and José González-Valdez would like to thank the Bioprocess Focus Group (0020209I13) of Tecnológico de Monterrey for its support.

Author Contributions

Conceptualization: Roberto F. Delgadillo, Timothy C. Mueser, Kathia Zaleta-Rivera, Lawrence J. Parkhurst.

Data curation: Roberto F. Delgadillo, Timothy C. Mueser.

Formal analysis: Roberto F. Delgadillo.

Funding acquisition: Roberto F. Delgadillo, José González-Valdez, Lawrence J. Parkhurst.

Investigation: Roberto F. Delgadillo, Timothy C. Mueser.

Methodology: Roberto F. Delgadillo, Timothy C. Mueser, Lawrence J. Parkhurst.

Project administration: Roberto F. Delgadillo, Lawrence J. Parkhurst.

Resources: Roberto F. Delgadillo.

Software: Roberto F. Delgadillo.

Supervision: Roberto F. Delgadillo, Timothy C. Mueser, Kathia Zaleta-Rivera, Katie A. Carnes, Lawrence J. Parkhurst.

Validation: Roberto F. Delgadillo, Timothy C. Mueser, Kathia Zaleta-Rivera, Katie A. Carnes, José González-Valdez.

Visualization: Roberto F. Delgadillo.

Writing – original draft: Roberto F. Delgadillo.

Writing – review & editing: Roberto F. Delgadillo, Timothy C. Mueser, Kathia Zaleta-Rivera, Katie A. Carnes, José González-Valdez, Lawrence J. Parkhurst.

References

1. Wilchek M, Bayer EA. Introduction to avidin-biotin technology. Methods Enzymol. 1990; 184 C:5–13.
2. Wilchek M. My life with affinity. Protein Sci. 2004; 11:3066–70.
3. Bayer EA, Wilchek M. The Use of the Avidin-Biotin Complex as a Tool in Molecular Biology. Methods Biochem Anal. 1980; 26:1–45. https://doi.org/10.1002/9780470110461.ch1 PMID: 7392958
4. Diamandis EP, Christopoulos TK. The biotin-(strept)avidin system: principles and applications in biotechnology. Clin Chem. 1991; 37:625–36. PMID: 2032315
5. Wilchek M, Bayer EA. The avidin-biotin complex in immunology. Immunol Today. 1984; 5:39–43. https://doi.org/10.1016/0167-5699(84)90027-6 PMID: 25291372
6. Orth RN, Clark TG, Craighead HG. Avidin-Biotin Micropatterning Methods for Biosensor Applications. Biomed Microdevices. 2003; 5:29–34.
7. Park KM, Murray J, Kim K. Ultrastable artificial binding pairs as a supramolecular latching system: A next generation chemical tool for proteomics. Acc Chem Res. 2017; 50:644–6. https://doi.org/10.1021/acs.accounts.6b00645 PMID: 28945411
8. Jurinke C, Van den Boom D, Collazo V, Lüchow A, Jacob A, Köster H. Recovery of Nucleic Acids from Immobilized Biotin-Streptavidin Complexes Using Ammonium Hydroxide and Applications in MALDI-Tof Mass Spectrometry. Anal Chem. 1997; 69:904–10. PMID: 9068275
9. Michalet X, Pinaud FF, Bentolila LA, Tsay JM, Doose S, Li JJ, et al. Quantum dots for live cells, in vivo imaging, and diagnostics. Science. 2005; 307:538–44. https://doi.org/10.1126/science.1104274 PMID: 15681376
10. Howarth M, Ting AY. Imaging proteins in live mammalian cells with biotin ligase and monovalent streptavidin. Nat Protoc. 2008; 3:534–45. https://doi.org/10.1038/nprot.2008.20 PMID: 18323822
11. Jain A, Cheng K. The principles and applications of avidin-based nanoparticles in drug delivery and diagnosis. J Control Release. 2017; 245:27–40. https://doi.org/10.1016/j.jconrel.2016.11.016 PMID: 27865853

12. Förster T, Energiewanderung Z, Von F. Zwischenmolekulare Energiewanderung und Fluoreszenz. Ann Phys. 1948; 437:55–75.
13. Bazin Préaudat, Trinquet Mathis. Homogeneous time resolved fluorescence resonance energy transfer using rare earth cryptates as a tool for probing molecular interactions in biology. Spectrochim acta Part A, Mol Biomol Spectrosc. 2001; 57:2197–211.
14. Cisbio. HTRF Glucagon Kit Protocol. Cisbio Appl Note. 2016.
15. Nørskov-Lauritsen L, Thomsen ARB, Bräuner-Osborne H. G protein-coupled receptor signaling analysis using homogenous time-resolved Förster resonance energy transfer (HTRF) technology. Int J Mol Sci. 2014; 15:2554–72. https://doi.org/10.3390/ijms15022554 PMID: 24531140
16. Morpurgo M, Radu A, Bayer EA, Wilchek M. DNA condensation by high-affinity interaction with avidin. J Mol Recognit. 2004; 17:558–66. https://doi.org/10.1002/jmr.689 PMID: 15386619
17. Kramer KJ, Morgan TD, Throne JE, Dowell FE, Bailey M, Howard JA. Transgenic avidin maize is resistant to storage insect pests. Nat Biotechnol. 2000; 18:670–4. https://doi.org/10.1038/76531 PMID: 10835608
18. Helppolainen SH, Nurminen KP, Määttä J a E, Halling KK, Slotte JP, Huhtala T, et al. Rhizavidin from Rhizobium etli: the first natural dimer in the avidin protein family. Biochem J. 2007; 405:397–405. https://doi.org/10.1042/BJ20070076 PMID: 17447892
19. Meir A, Helppolainen SH, Podoly E, Nordlund HR, Hytönen VP, Määttä JA, et al. Crystal Structure of Rhizavidin: Insights into the Enigmatic High-Affinity Interaction of an Innate Biotin-Binding Protein Dimer. J Mol Biol. 2009; 386:379–90. https://doi.org/10.1016/j.jmb.2008.11.061 PMID: 19111749
20. Takakura Y, Tsunashima M, Suzuki J, Usami S, Kakuta Y, Okino N, et al. Tamavidins—Novel avidin-like biotin-binding proteins from the Tamogitake mushroom. FEBS J. 2009; 276:1383–97. https://doi.org/10.1111/j.1742-4658.2009.06879.x PMID: 19187241
21. Määttä JA, Helppolainen SH, Hytönen VP, Johnson MS, Kulomaa MS, Airenne TT, et al. Structural and functional characteristics of xenavidin, the first frog avidin from Xenopus tropicalis. BMC Struct Biol. 2009; 9:63. https://doi.org/10.1186/1472-6807-9-63 PMID: 19788720
22. Helppolainen SH, Määttä JAE, Halling KK, Slotte JP, Hytönen VP, Jänis J, et al. Bradavidin II from Bradyrhizobium japonicum: A new avidin-like biotin-binding protein. Biochim Biophys Acta—Proteins Proteomics. 2008; 1784:1002–10.
23. Nordlund HR, Hytönen VP, Laitinen OH, Kulomaa MS. Novel avidin-like protein from a root nodule symbiotic bacterium, Bradyrhizobium japonicum. J Biol Chem. 2005; 280:13250–5. https://doi.org/10.1074/jbc.M414336200 PMID: 15695809
24. Keinänen RA, Wallén MJ, Kristo PA, Laukkanen MO, Toimela TA, Helenius MA, et al. Molecular cloning and nucleotide sequence of chicken avidin-related genes 1–5. Eur J Biochem. 1994; 220:615–21. PMID: 8125122
25. Hytönen VP, Määttä JAE, Kidron H, Halling KK, Hörhä J, Kulomaa T, et al. Avidin related protein 2 shows unique structural and functional features among the avidin protein family. BMC Biotechnol. 2005; 5:28. https://doi.org/10.1186/1472-6750-5-28 PMID: 16212654
26. Prizant M, Eisenberg-Domovich Y, Hytönen VP, Kulomaa MS, Wilchek M, Bayer EA, et al. Factors Dictating the Pseudocatalytic Efficiency of Avidins. J Mol Biol. 2006; 358:754–63. https://doi.org/10.1016/j.jmb.2006.02.044 PMID: 16546211
27. Huberman T, Eisenberg-Domovich Y, Gitlin G, Kulik T, Bayer EA, Wilchek M, et al. Chicken avidin exhibits pseudo-catalytic properties. Biochemical, structural, and electrostatic consequences. J Biol Chem. 2001; 276:32031–9. https://doi.org/10.1074/jbc.M102018200 PMID: 11395489
28. Hayouka R, Eisenberg-Domovich Y, Hytönen VP, Määttä JAE, Nordlund HR, Kulomaa MS, et al. Critical importance of loop conformation to avidin-enhanced hydrolysis of an active biotin ester. Acta Crystallogr Sect D Biol Crystallogr. 2008; 64:302–8.
29. Laitinen OH, Hytönen VP, Ahlroth MK, Pentikäinen OT, Gallagher C, Nordlund HR, et al. Chicken avidin-related proteins show altered biotin-binding and physico-chemical properties as compared with avidin. Biochem J. 2002; 363:609–17. PMID: 11964162
30. Niskanen EA, Hytönen VP, Grapputo A, Nordlund HR, Kulomaa MS, Laitinen OH. Chicken genome analysis reveals novel genes encoding biotin-binding proteins related to avidin family. BMC Genomics. 2005; 6:41. https://doi.org/10.1186/1471-2164-6-41 PMID: 15777476
31. Hytönen VP, Nyholm TKM, Pentikäinen OT, Vaarno J, Porkka EJ, Nordlund HR, et al. Chicken Avidin-related Protein 4/5 Shows Superior Thermal Stability when Compared with Avidin while Retaining High Affinity to Biotin. J Biol Chem. 2004; 279:9337–43. https://doi.org/10.1074/jbc.M310989200 PMID: 14660583

32. Livnah O, Bayer EA, Wilchek M, Sussman JL. Three-dimensional structures of avidin and the avidin-biotin complex. Proc Natl Acad Sci. 1993; 90:5076–80. https://doi.org/10.1073/pnas.90.11.5076 PMID: 8506353

33. Donovan JW, Ross KD. Increase in the Stability of Avidin Produced by Binding of Biotin. a Differential Scanning Calorimetric Study of Denaturation by Heat. Biochemistry. 1973; 12:512–7. PMID: 4683493

34. Laitinen OH, Nordlund HR, Hytönen VP, Uotila STH, Marttila AT, Savolainen J, et al. Rational design of an active avidin monomer. J Biol Chem. 2003.

35. Green NM. The use of [14C]biotin for kinetic studies and for assay. Biochem J. 1963; 89:585–91. http://www.pubmedcentral.nih.gov/articlerender.fcgi?artid=1202466&tool=pmcentrez&rendertype=abstract. PMID: 14101979

36. Wayment JR, Harris JM. Biotin-avidin binding kinetics measured by single-molecule imaging. Anal Chem. 2009; 81:336–42. https://doi.org/10.1021/ac801818t PMID: 19117461

37. Srisa-Art M, DeMello AJ, Edel JB. High-throughput DNA droplet assays using picoliter reactor volumes. Anal Chem. 2007; 79:6682–9. https://doi.org/10.1021/ac070987o PMID: 17676925

38. Srisa-Art M, Dyson EC, DeMello AJ, Edel JB. Monitoring of real-time streptavidin-biotin binding kinetics using droplet microfluidics. Anal Chem. 2008; 80:7063–7. https://doi.org/10.1021/ac801199k PMID: 18712935

39. Hyre DE, Le Trong I, Merritt EA, Eccleston JF, Green NM, Stenkamp RE, et al. Cooperative hydrogen bond interactions in the streptavidin-biotin system. Protein Sci. 2006; 15:459–67. https://doi.org/10.1110/ps.051970306 PMID: 16452627

40. Green NM. Spectrophotometric Determination of Avidin and Biotin. Methods Enzymol. 1970; 18:418–24.

41. Livnah O, Bayer EA, Wilchek M, Sussman JL. The structure of the complex between avidin and the dye, 2-(4'-hydroxyazobenzene) benzoic acid (HABA). FEBS Lett. 1993; 328:165–8. PMID: 8344421

42. Delgadillo RF, Whittington JDE, Parkhurst LK, Parkhurst LJ. The TATA-binding protein core domain in solution variably bends TATA sequences via a three-step binding mechanism. Biochemistry. 2009; 48:1801–9. https://doi.org/10.1021/bi8018724 PMID: 19199812

43. Pihan E, Delgadillo RF, Tonkin ML, Pugnière M, Lebrun M, Boulanger MJ, et al. Computational and biophysical approaches to protein-protein interaction inhibition of Plasmodium falciparum AMA1/RON2 complex. J Comput Aided Mol Des. 2015; 29:525–39. https://doi.org/10.1007/s10822-015-9842-7 PMID: 25822046

44. Whittington JDE, Delgadillo RF, Attebury TJ, Parkhurst LK, Daugherty MA, Parkhurst LJ. TATA-binding protein recognition and bending of a consensus promoter are protein species dependent. Biochemistry. 2008; 47:7264–73. https://doi.org/10.1021/bi800139w PMID: 18553934

45. Delgadillo RF, Parker ML, Lebrun M, Boulanger MJ, Douguet D. Stability of the Plasmodium falciparum AMA1-RON2 Complex Is Governed by the Domain II (DII) Loop. PLoS One. 2016; 11.

46. Delgadillo RF, Parkhurst LJ. Spectroscopic properties of fluorescein and rhodamine dyes attached to DNA. Photochem Photobiol. 2010; 86:261–72. https://doi.org/10.1111/j.1751-1097.2009.00663.x PMID: 20003160

47. Hytönen VP, Määttä JAE, Niskanen EA, Huuskonen J, Helttunen KJ, Halling KK, et al. Structure and characterization of a novel chicken biotin-binding protein A (BBP-A). BMC Struct Biol. 2007;7. https://doi.org/10.1186/1472-6807-7-7

48. Giblin DE. A modular instrument for the measurement of transient circular dichroism, fluorescence polarization and emission anisotropy. University of Nebraska-Lincoln; 1978.

49. Parker CA, Rees WT. Correction of fluorescence spectra and measurement of fluorescence quantum efficiency. Analyst. 1960; 85:587. https://doi.org/10.1039/an9608500587

50. Crosby GA, Demas JN. Measurement of photoluminescence quantum yields. Review. J Phys Chem. 1971; 75:991–1024. https://doi.org/10.1021/j100678a001

51. Mueser TC. Steady state fluorescence and fluorescence anisotropy studies of ligand binding and kinetics. University of Nebraska-Lincoln; 1989.

52. Foss SD. A Method of Exponential Curve Fitting by Numerical Integration. Biometrics. 1970; 26:815–21. https://doi.org/10.2307/2528726

53. Görisch H, Goss DJ, Parkhurs LJ. Kinetics of Ribosome Dissociation and Subunit Association Studied in a Light-Scattering Stopped-Flow Apparatus. Biochemistry. 1976; 15:5743–53. PMID: 795460

54. Parkhurst KM, Brenowitz M, Parkhurst LJ. Simultaneous binding and bending of promoter DNA by the TATA binding protein: Real time kinetic measurements. Biochemistry. 1996; 35:7459–65. https://doi.org/10.1021/bi9530301 PMID: 8652523

55. Otto MR, Lillo MP, Beechem JM. Resolution of multiphasic reactions by the combination of fluorescence total-intensity and anisotropy stopped-flow kinetic experiments. Biophys J. 1994; 67:2511–21. https://doi.org/10.1016/S0006-3495(94)80741-6 PMID: 7696490

56. Bucci E, Steiner RF. Anisotropy decay of fluorescence as an experimental approach to protein dynamics. Biophys Chem. 1988; 30:199–224. PMID: 3061490

57. Cantor C. R., and Schimmel PR. Techniques for the Study of Biological Structure and Function (Pt. 2). First. San Francisco.: W.H. Freeman and Company; 1980.

58. Parkhurst LJ, Parkhurst KM, Powell R, Wu J, Williams S. Time-resolved fluorescence resonance energy transfer studies of DNA bending in double-stranded oligonucleotides and in DNA-protein complexes. Biopolymers. 2002; 61:180–200. https://doi.org/10.1002/bip.10138 PMID: 11987180

59. Lipari G, Szabo A. Effect of librational motion on fluorescence depolarization and nuclear magnetic resonance relaxation in macromolecules and membranes. Biophys J. 1980; 30:489–506. https://doi.org/10.1016/S0006-3495(80)85109-5 PMID: 7260284

60. GREEN NM. AVIDIN. 3. THE NATURE OF THE BIOTIN-BINDING SITE. Biochem J. 1963; 89:599–609. https://doi.org/10.1042/bj0890599 PMID: 14101981

61. Sinha B. K., and Chignell CF. The synthesis and use of spin-labeled analogs of biotin in the study of avidin. Methods Enzymol. 1979; 62:295–308. PMID: 220506

62. Bayer EA, Wilchek M. Biotin-binding Proteins: Overview and Prospects. Methods Enzymol. 1990; 184 C:49–51.

63. Perutz MF, Ladner JE, Simon SR, Chien H. Influence of globin structure on the state of the heme. I. Human deoxyhemoglobin. Biochemistry. 1974; 13:2163–73. PMID: 4826890

64. Parkhurst LJ, Goss DJ, Perutz MF, Parkhurst LJ, Goss DJ, Perutz MF. Kinetic and Equilibrium Studies on the Role of the β-147 Histidine in the Root Effect and Cooperativity in Carp Hemoglobin. Biochemistry. 1983; 22:5401–9.

65. Hiller Y, Gershoni JM, Bayer EA, Wilchek M. Biotin binding to avidin. Oligosaccharide side chain not required for ligand association. Biochem J. 1987; 248:167–71. https://doi.org/10.1042/bj2480167 PMID: 3435435

66. Qureshi MH, Yeung JC, Wu SC, Wong SL. Development and Characterization of a Series of Soluble Tetrameric and Monomeric Streptavidin Muteins with Differential Biotin Binding Affinities. J Biol Chem. 2001; 276:46422–8. https://doi.org/10.1074/jbc.M107398200 PMID: 11584006

67. John W. Moore RGP. Kinetics and Mechanism. Third. Wiley Interscience; 1981.

68. Piran U, Riordan WJ. Dissociation rate constant of the biotin-streptavidin complex. J Immunol Methods. 1990; 133:141–3. PMID: 2212686

69. Reczek EE, James MF, Brems H. Engineered single-chain dimeric streptavidins with an unexpected strong preference for biotin-4-fluorescein. Proc Natl Acad Sci. 2005.

70. Buranda T, Jones GM, Nolan JP, Keij J, Lopez GP, Sklar LA. Ligand Receptor Dynamics at Streptavidin-Coated Particle Surfaces: A Flow Cytometric and Spectrofluorimetric Study. J Phys Chem B. 1999; 103:3399–410. https://doi.org/10.1021/jp983842h

71. Wu Y, Simons PC, Lopez GP, Sklar LA, Buranda T. Dynamics of fluorescence dequenching of ostrich-quenched fluorescein biotin: A multifunctional quantitative assay for biotin. Anal Biochem. 2005; 342:221–8. https://doi.org/10.1016/j.ab.2005.03.046 PMID: 15913533

72. De Paris R, Strunz T, Oroszlan K, Güntherodt H-J, Hegner M. Force Spectroscopy and Dynamics of the BiotinAvidin Bond Studied by Scanning Force Microscopy. Single Mol. 2000; 1:285–90.

73. Connors KA. Chemical Kinetics: The Study of Reaction Rates in Solution. New York: VCH Publishers, Inc; 1990.

74. González M, Argaraña CE, Fidelio GD. Extremely high thermal stability of streptavidin and avidin upon biotin binding. Biomol Eng. 1999; 16:67–72. PMID: 10796986

75. Celej MS, Montich GG, Fidelio GD. Conformational flexibility of avidin: The influence of biotin binding. Biochem Biophys Res Commun. 2004; 325:922–7. https://doi.org/10.1016/j.bbrc.2004.10.118 PMID: 15541378

76. Green N. Thermodynamics of the binding of biotin and some analogues by avidin. Biochem J. 1966; 101:774–80. https://doi.org/10.1042/bj1010774 PMID: 16742458

77. Stjurkuusk J, Wadso I. Thermochemistry of the Avidin-Biotin Reaction Calorimetric Equipment and Procedure For the protein-binding experiments an LKB. Eur J Biochem. 1972; 28:438–41. PMID: 5079946

78. Swamy MJ. Thermodynamic analysis of biotin binding to avidin. A high sensitivity titration calorimetric study. Biochem Mol Biol Int. 1995; 36:219–25. PMID: 7663418

79. Waner MJ, Mascotti DP. A simple spectrophotometric streptavidin-biotin binding assay utilizing biotin-4-fluorescein. J Biochem Biophys Methods. 2008; 70:873–7. https://doi.org/10.1016/j.jbbm.2007.06.001 PMID: 17669504

80. Klumb LA, Chu V, Stayton PS. Energetic roles of hydrogen bonds at the ureido oxygen binding pocket in the streptavidin-biotin complex. Biochemistry. 1998; 37:7657–63. https://doi.org/10.1021/bi9803123 PMID: 9601024

81. Stayton PS, Freitag S, Klumb LA, Chilkoti A, Chu V, Penzotti JE, et al. Streptavidin-biotin binding energetics. Biomol Eng. 1999; 16:39–44. PMID: 10796983

82. Hyre DE, Le Trong I, Freitag S, Stenkamp RE, Stayton PS. Ser45 plays an important role in managing both the equilibrium and transition state energetics of the streptavidin-biotin system. Protein Sci. 2000; 9:878–85. https://doi.org/10.1110/ps.9.5.878 PMID: 10850797

83. Weber PC, Wendoloski JJ, Pantoliano MW, Salemme FR. Crystallographic and Thermodynamic Comparison of Natural and Synthetic Ligands Bound to Streptavidin. J Am Chem Soc. 1992; 114:3197–200.

84. Weber P. C., Pantoliano M. W., and Salemme R. General Medical Applications of Structure-Aided Design. Crystallographic and Thermodynamics Comparison of Structurally Diverse Molecules Binding to Strepavidin. Acta Cryst. 1995; D51:590–6.

85. Sjöback R, Nygren J, Kubista M, Sjback R, Nygren J, Kubista M. Absorption and fluorescence properties of fluorescein. Spectrochim Acta Part A. 1995; 51:L7–21.

86. Sjöback R, Nygren J, Kubista M. Characterization of Fluorescein–Oligonucleotide Conjugates and Measurement of Local Electrostatic Potential. Biopolymers. 1998; 46:445–53. https://doi.org/10.1002/(SICI)1097-0282(199812)46:7<445::AID-BIP2>3.0.CO;2-5 PMID: 9838871

87. Sjoback R, Nygren J, Kubista M. Characterization of fluorescein-oligonucleotide conjugates and measurement of local electrostatic potential. Doktorsavhandlingar vid Chalmers Tek Hogsk. 1999:445–53.

88. Parkhurst LJ. Near-Infrared Applications in Biotechnology. Practical Spectroscopy Series (R. Raghavachari, Ed). New York: Marcel Dekker, Inc; 2001. p. 5–33.

89. General IJ, Dragomirova R, Meirovitch H. Absolute free energy of binding of avidin/biotin, revisited. J Phys Chem B. 2012; 116:6628–36. https://doi.org/10.1021/jp212276m PMID: 22300239

90. Kada G, Kaiser K, Falk H, Gruber HJ. Rapid estimation of avidin and streptavidin by fluorescence quenching or fluorescence polarization. Biochim Biophys Acta—Gen Subj. 1999; 1427:44–8.

91. Oregan B, Gratzel M. A Low-cost, High-efficiency Solar Cell Based on Dye-sensitized Colloidal TiO2 Films. Nature. 1991; 353:737–40.

92. McGehee MD. Applied physics. Paradigm shifts in dye-sensitized solar cells. Science. 2011; 334:607–8. https://doi.org/10.1126/science.1212818 PMID: 22053034

93. Ito S. Investigation of Dyes for Dye-Sensitized Solar Cells: Ruthenium-Complex Dyes, Metal-Free Dyes, Metal-Complex Porphyrin Dyes and Natural Dyes. InTech. 2011;20–48.

94. Zauner D, Taskinen B, Eichinger D, Flattinger C, Ruttmann B, Knoglinger C, et al. Regenerative biosensor chips based on switchable mutants of avidin—A systematic study. Sensors Actuators B Chem. 2016; 229:646–54.

95. Pollheimer P, Taskinen B, Scherfler A, Gusenkov S, Creus M, Wiesauer P, et al. Reversible biofunctionalization of surfaces with a switchable mutant of avidin. Bioconjug Chem. 2013; 24:1656–68. https://doi.org/10.1021/bc400087e PMID: 23978112

96. Lakowicz JR. Principles of fluorescence spectroscopy. 2006.